J. Fluid Mech. (2001), *vol.* 444, *pp.* 257–297. Printed in the United Kingdom

Chaotic advection in three-dimensional stationary vortex-breakdown bubbles: Šil'nikov's chaos and the devil's staircase

By FOTIS SOTIROPOULOS, YIANNIS VENTIKOS† AND TAHIRIH C. LACKEY

School of Civil and Environmental Engineering, Georgia Institute of Technology, Atlanta, GA 30332–0355, USA

(Received 2 October 1999 and in revised form 19 January 2001)

We study the motion of non-diffusive, passive particles within steady, three-dimensional vortex breakdown bubbles in a closed cylindrical container with a rotating bottom. The velocity fields are obtained by solving numerically the three-dimensional Navier–Stokes equations. We clarify the relationship between the manifold structure of axisymmetric (ideal) vortex breakdown bubbles and those of the three-dimensional real-life (laboratory) flow fields, which exhibit chaotic particle paths. We show that the upstream and downstream fixed hyperbolic points in the former are transformed into spiral-out and spiral-in saddles, respectively, in the latter. Material elements passing repeatedly through the two saddle foci undergo intense stretching and folding, leading to the growth of infinitely many Smale horseshoes and sensitive dependence on initial conditions via the mechanism discovered by Šil'nikov (1965). Chaotic Šil'nikov orbits spiral upward (from the spiral-in to the spiral-out saddle) around the axis and then downward near the surface, wrapping around the toroidal region in the interior of the bubble. Poincaré maps reveal that the dynamics of this region is rich and consistent with what we would generically anticipate for a mildly perturbed, volume-preserving, three-dimensional dynamical system (MacKay 1994; Mezić & Wiggins 1994*a*). Nested KAM-tori, cantori, and periodic islands are found embedded within stochastic regions. We calculate residence times of upstream-originating non-diffusive particles and show that when mapped to initial release locations the resulting maps exhibit fractal properties. We argue that there exists a Cantor set of initial conditions that leads to arbitrarily long residence times within the breakdown region. We also show that the emptying of the bubble does not take place in a continuous manner but rather in a sequence of discrete bursting events during which clusters of particles exit the bubble at once. A remarkable finding in this regard is that the rate at which an initial population of particles exits the breakdown region is described by the devil's staircase distribution, a fractal curve that has been already shown to describe a number of other chaotic physical systems.

1. Introduction

The notion that the vortex breakdown bubbles observed in laboratory visualization experiments (e.g. Sarpkaya 1971; Faler & Leibovich 1977) could exhibit chaotic

† Present address: Laboratory for Thermodynamics in Emerging Technologies, Swiss Federal Institute of Technology, ML K17, ETH–Zentrum, Zurich, CH-8092, Switzerland.

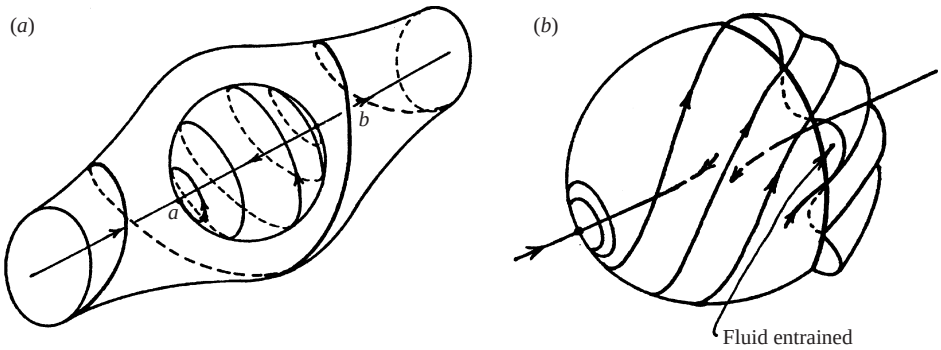

FIGURE 1. Bubble-type vortex breakdown. (*a*) The unperturbed manifolds, and (*b*) the resulting manifold splitting as a consequence of perturbing the velocity field as envisaged by Holmes (1984).

particle paths was first put forth by Holmes (1984) some sixteen years ago. Starting from a steady, axisymmetric, vortex breakdown bubble, Holmes described a scenario via which certain invariant manifolds connecting the upstream and downstream fixed hyperbolic points of the axisymmetric flow could break down under the action of an arbitrarily small, time-periodic, non-axisymmetric mode. As a consequence, the bubble-like streamsurface, which in the axisymmetric flow delineates the re-circulating vortex breakdown region from the outer flow, is no longer invariant, allowing fluid to be exchanged between the bubble and the outer flow in a complex, three-dimensional manner (see figure 1). Holmes (1984) further argued that the resulting three-dimensional flow could be fundamentally different from its axisymmetric counterpart, even though, in an Eulerian sense, the difference between them is an arbitrarily small perturbation – a similar point was also made by Leibovich (1984) while commenting on the relation between solutions of the axisymmetric Navier–Stokes equations and the nearly axisymmetric vortex breakdown flows observed in the laboratory. Holmes went on to describe a spatially chaotic, three-dimensional flow in which upstream originating particles enter the bubble through its downstream end, circulate arbitrarily many times, and finally exit, to continue downstream (Holmes 1984).

Some experimental evidence that supports, at least indirectly, Holmes's conjectures was reported by Driscoll and co-workers (Chen & Driscoll 1988; Feikema, Chen & Driscoll 1990) from a series of laboratory experiments with swirl-stabilized flames. Driscoll's work demonstrated that vortex breakdown could greatly enhance the overall fuel–air mixing efficiency leading to complete combustion and short flame lengths. Although the possibility of chaotic mixing was not explicitly discussed in these papers, the description of the structure of the breakdown region and the observed mixing mechanisms is especially revealing. For instance, while discussing their flow visualization photographs Chen & Driscoll (1988) comment that '... both fuel and air enter the recirculation vortex primarily near the downstream region of the vortex', and that the breakdown region acts to '... entrain and stretch the ligaments of fuel, and thereby increase the fuel/air contact area'. Furthermore, they remark that mixing occurs '... due to larger-scale rather than small-scale motions'. Clearly, therefore, the mixing processes described by Chen & Driscoll (1988) in conjunction with the dramatic enhancement of mixing efficiency they reported suggest a chaotic large-scale flow field in which material elements are stretched exponentially.

In spite of a large and constantly growing body of literature dedicated to the study of vortex breakdown, the Lagrangian dynamics of the phenomenon, which

need to be elucidated before the mixing mechanisms observed in the laboratory can be explained, have been largely unexplored. The only study that emphasized the Lagrangian characteristics of vortex breakdown flow fields was the work of Lopez & Perry (1992) who studied numerically the flow in a closed cylindrical container with a rotating lid. They demonstrated how concepts from dynamical systems could be employed to study the onset of Lagrangian chaos within oscillatory vortex breakdown bubbles. Their work, however, assumed axisymmetric flow and, thus, could neither resolve nor explain the asymmetries observed in all laboratory visualization experiments of vortex breakdown structures in this flow (see the recent work of Spohn, Mory & Hopfinger 1998 and subsequent discussion). Furthermore, the assumption of axisymmetric flow – which, by definition, leads to integrable particle paths in the steady flow regime – precluded the possibility of steady, spatially chaotic vortex breakdown flow fields. Although in recent years a number of three-dimensional, unsteady simulations of vortex breakdown have also been reported in the literature (e.g. Spall & Gatski 1991; Tromp & Beran 1997; Lucas 1997), they have primarily emphasized the vorticity dynamics of the phenomenon and have not attempted to explore its Lagrangian characteristics.

We have recently reported three-dimensional numerical simulations of vortex breakdown in a closed cylindrical container with a rotating lid and succeeded, for the first time, in reproducing with remarkable accuracy the Lagrangian features of the phenomenon observed in the laboratory (Sotiropoulos & Ventikos 2001). Before we proceed with a summary of these findings, which have motivated the present contribution, it is important to briefly review previous experimental and computational work on the container flow. Although this flow has been studied extensively in the past both numerically and experimentally (e.g. Lopez 1990; Brown & Lopez 1990; Watson & Neitzel 1996; Gelfgat, Bar-Yoseph & Solan 1996; Tsitvertblit & Kit 1998; Stevens, Lopez & Cantwell 1999; Brons, Voigt & Sorensen 1999), its fundamental nature (axisymmetric or three-dimensional) has been, at least until recently, the subject of considerable controversy. As we discuss in Sotiropoulos & Ventikos (2001) and further elaborate in the remainder of this paper, the key to resolving the various conflicting points of view that have appeared in the literature is Holmes's conjecture concerning the potentially dramatic effect an arbitrarily small, non-axisymmetric mode could have on the Lagrangian dynamics of an axisymmetric flow.

1.1. *Previous studies of vortex breakdown in a cylindrical container with a rotating lid*

The first comprehensive flow visualization experiments for the container flow were carried out by Escudier (1984), who concluded that the visualized breakdown bubbles are axisymmetric, at least within the steady flow regime. Based on this finding, Escudier (1984, 1988) went on to argue that the fundamental form of vortex breakdown is the axisymmetric, bubble-type mode and that the emergence of the highly three-dimensional spiral mode is the result of non-axisymmetric instabilities of the basic bubble form. There are, however, some interesting features in Escudier's visualization photographs that are not entirely consistent with an axisymmetric flow. These include: (i) the observed asymmetric spiralling of the dye filament just prior to the inception of the breakdown bubble; (ii) the formation of distinct asymmetric folds at the downstream end of the bubbles; and (iii) the presence of a considerable amount of dye in the interior of the bubbles – a feature that cannot be readily explained by adopting the concept of a closed axisymmetric bubble. Spohn, Mory & Hopfinger (1993) were the first to raise some questions concerning the symmetry of the flow by pointing out the persistence of asymmetric spirals prior to the bubble inception in

their experiment and suggesting that details of the flow surrounding the container axis need also be examined to clarify this issue. Motivated by these comments, Hourigan, Graham & Thompson (1995) carried out experiments and axisymmetric numerical computations and argued that the apparent asymmetries are artifacts of the flow visualization technique and that the actual flow remains perfectly axisymmetric. In a more recent study, Stevens, Lopez & Cantwell (1999), who focused on the transition from the steady to the oscillatory flow regime, observed in their flow visualizations a spiral-like precession of the upstream fixed hyperbolic point of the breakdown bubble, which they also attributed to imperfections of the visualization technique. It should be emphasized that in all these studies the arguments concerning the axial symmetry of the flow were reinforced by the fact that axisymmetric computations reproduced the general flow patterns, and the evolution of these patterns with Reynolds number and container aspect ratio, observed in the laboratory both in the steady and unsteady flow regimes (Lopez 1990; Gelfgat *et al.* 1996; Stevens *et al.* 1999). Of course, these computations could neither reproduce the asymmetric folds at the downstream end of the laboratory vortex breakdown bubbles nor explain the process via which large amounts of dye in these experiments penetrate a stationary, axisymmetric, recirculating flow region.

The first experiment that attempted to study the origin and nature of the asymmetries of the container flow in detail was reported by Spohn *et al.* (1998) who visualized the vortex breakdown bubbles using a variety of dye and other tracer injection techniques. Their results establish clearly that there exists a range of Reynolds numbers within which the on-axis vortex breakdown bubbles are stationary, open, and highly asymmetric at their downstream end. Spohn *et al.* (1998) traced the origin of the asymmetries to the emergence of spiral, asymmetric, separation lines inside the cylindrical sidewall boundary layer.

Our recent numerical computations (Sotiropoulos & Ventikos 2001) clarified the findings of Spohn *et al.* (1998), established clearly the three-dimensional structure of the container flow, and explained the link between the three-dimensional sidewall boundary layer and the asymmetries of the on-axis breakdown bubbles. More specifically, we showed that the sidewall boundary layer loses stability to three-dimensional disturbances in the form of counter-rotating pairs of spiral vortices (see also the extensive discussion in Sotiropoulos & Ventikos 1998). Although coherent spiral vortices were found for Reynolds numbers well within the unsteady flow regime, traces of the three-dimensional instability were also present in the steady flow fields. In agreement with the experimental findings of Spohn *et al.* (1998), our computations revealed that in the steady regime the flow leaving the sidewall boundary layer does not enter the stationary-cover Ekman layer axisymmetrically but rather forms distinct azimuthal clusterings. We demonstrated the accuracy of our computations by reproducing numerically Lagrangian images of the breakdown bubbles that are in remarkable agreement with available flow visualization photographs. Moreover, we showed that the computed vortex breakdown flow fields exhibit extreme sensitivity to initial conditions, as initially nearby particles diverge exponentially in time. This finding, which establishes the chaotic nature of the flow, confirms the general scenario described by Holmes (1984) but further suggests that even a stationary, non-axisymmetric mode could drastically alter the Lagrangian dynamics of a steady, axisymmetric flow. We should emphasize that in the vicinity of the breakdown bubbles our computed three-dimensional flow fields are, in terms of Eulerian comparison measures (for example contours of velocity and/or vorticity components), very similar to those obtained when solving the axisymmetric equations for the same set of governing parameters.

Even though, therefore, the asymmetric mode in the three-dimensional flow fields is small, it has a profound impact on the Lagrangian characteristics of the flow: it causes the spiral-like deflection of the on-axis filament just upstream of the front stagnation point of the bubble and transforms the downstream fixed hyperbolic point of the axisymmetric flow into a spiral-in saddle through which fluid is exchanged between the interior of the bubble and the outer flow.

1.2. *Previous studies of chaotic advection*

Our finding concerning the chaotic nature of the flow in the interior of vortex breakdown bubbles places the container problem among a handful of experimentally realizable, and numerically reproducible, three-dimensional flows that can be used to study stirring (and mixing if molecular diffusion is taken into account) by chaotic advection. This phenomenon manifests itself in the trajectories of passive Lagrangian markers that are advected by a flow field of very simple Eulerian structure (Aref 1984). Chaotic advection is the only mechanism for enhancing mixing in non-turbulent flows and is, therefore, important in a number of industrial, physiological, and geophysical applications (Aref 1999). Over the last fifteen years, a large number of experimental (e.g. Chaiken *et al.* 1986; Leong & Ottino 1989; Swanson & Ottino 1990; Rothstein, Henry & Gollub 1999) and numerical (e.g. Aref 1984; Chien, Rising & Ottino 1986; Khakhar, Rising & Ottino 1986; Rom-Kedar, Leonard & Wiggins 1990; Ghosh, Leonard & Wiggins 1998) studies of idealized two-dimensional flows have contributed considerably to our understanding of chaotic stirring. These studies clarified and solidified the links between dynamical systems, topological fluid mechanics, and chaotic advection and led to a rigorous theoretical framework for studying chaotic mixing in two dimensions (see Beige, Leonard & Wiggins 1994 for a comprehensive review). However, considerably less progress has been made in the study of three-dimensional flows exhibiting chaotic advection, even though the very first example of chaotic advection was for a steady, three-dimensional flow (Arnold 1965; Hénon 1966). A significant obstacle in that regard is the lack of test-bed, three-dimensional flow fields of engineering relevance that are amenable to both experimental and numerical investigations (Fountain, Khakhar & Ottino 1998).

Most of the existing three-dimensional studies have employed mathematical flow models, such the ABC flow (Dombre *et al.* 1986), Beltrami flow in a sphere (Zheligovsky 1993), the Chandrashekar flow (Holm & Kimura 1991), and steady Stokes flow within a spherical drop (Bajer & Moffatt 1990; Stone, Nadim & Strogatz 1991; Kroujiline & Stone 1999). Studies with experimentally realizable, steady, three-dimensional flow fields have also been reported. Khakhar, Frajione & Ottino (1987) and Kusch & Ottino (1992) studied chaotic advection in a partitioned-pipe mixer. Jones, Thomas & Aref (1989) proposed a twisted-pipe configuration, which exhibits chaotic particle paths. Ashwin & King (1995) studied the Lagrangian dynamics of Taylor vortex flow between eccentric cylinders, while Ashwin & King (1997), Rudolph, Shinbrot & Lueptow (1998), and Rudman (1998) investigated non-axisymmetric Taylor–Couette flows between concentric cylinders. Hobbs & Muzzio (1997, 1998) studied in detail chaotic advection in a straight, helical static mixer. Fountain *et al.* (1998) and Fountain, Khakhar, Mezić & Ottino (2000) were the first to construct experimental Poincaré sections for a steady, three-dimensional creeping flow in an idealized mixing tank. Experimentally realizable, three-dimensional, unsteady flows have been investigated by Cartwright, Feingold & Piro (1996), Mezić, Leonard & Wiggins (1998), and Anderson *et al.* (1999).

Important ideas for developing the theoretical framework for the study of chaotic

advection in three-dimensional flows have been put forth by Holmes (1984), Feingold, Kadanoff & Piro (1988), MacKay (1994), and Mezić & Wiggins (1994). Haller & Mezić (1998) and Yannacopoulos *et al.* (1998) have taken some of these ideas further to propose Eulerian diagnostics that link the physics of the flow with the motion of particles. More recently, Mezić (2001) put forth a theory that links chaotic transport in three-dimensional wall-bounded flows with the thickness of the wall boundary layers.

1.3. *Outline of the present contribution*

In this work we employ Lagrangian particle tracking, tools from dynamical systems, and concepts from fractal geometry to conduct a comprehensive investigation of chaotic advection in the interior of the stationary vortex breakdown bubbles that occur along the axis of the container configuration. The three-dimensional flow fields are those obtained by Sotiropoulos & Ventikos (2001) who solved numerically the unsteady, three-dimensional Navier–Stokes equations using a second-order-accurate finite-volume method. Trajectories of passive, non-diffusive particles are calculated by employing a fourth-order-accurate Runge–Kutta method along with a tri-linear spatial interpolation technique. In § 2 we outline the numerical methods we employ to obtain the velocity fields and calculate the particle paths. In § 3 we compare our numerical computations with the laboratory visualizations of Spohn *et al.* (1998) and discuss some numerical issues we had to overcome in order to reproduce vortex-breakdown flow fields that exhibit chaotic dynamics. In § 4 we discuss the three-dimensional topology of the flow and argue that the mechanism discovered by Šil'nikov (1965) is responsible for destroying the invariance of the bubble-like surface and for the chaotic stirring of upstream originating particles within the breakdown region. In § 5 we demonstrate the three-dimensional stretching and folding of material elements, establish rigorously the exponential growth of length of material lines, and illustrate the chaotic stirring of Lagrangian markers. In § 6 we explore the dynamics of the flow in the interior of steady vortex breakdown bubbles by constructing Poincaré sections for a variety of initial conditions. We uncover and discuss in detail very rich and remarkably complex dynamics characterized by the presence of nested KAM-tori, cantori, and periodic islands surrounded by regions of chaotic motion. In § 7 we calculate residence times of non-diffusive particles within the breakdown region and argue that there exists a Cantor set of initial conditions that leads to arbitrarily long residence times. In § 8 we clarify the emptying process of breakdown bubbles and show that the rate at which particles exit is described by the devil's staircase curve. The fractal nature of this curve is established rigorously by computing the fractal dimension of the Cantor set associated with its construction. Finally in § 9 we comment on the implications and significance of our findings and outline areas for future research.

2. Problem formulation and numerical details

Consider a cylinder of radius R and length H filled with an incompressible Newtonian fluid of constant density ρ and kinematic viscosity ν. One endwall of the cylinder is rotated at a constant angular velocity Ω while the opposite endwall is held stationary (see figure 2). The two non-dimensional parameters governing the flow within this cylinder are the aspect ratio, H/R, and the Reynolds number $Re = \Omega R^2/\nu$. The flow generated by the rotating endwall is governed by the unsteady, three-dimensional, incompressible Navier–Stokes equations.

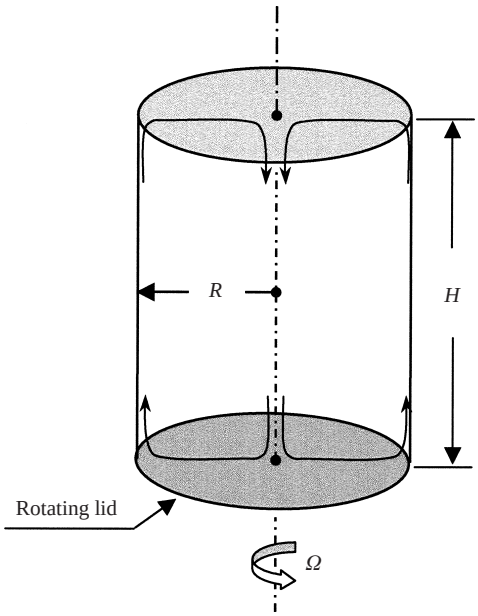

FIGURE 2. A schematic of the cylindrical container problem.

A detailed description of the numerical method we employ to solve the Navier–Stokes equations can be found in Sotiropoulos & Ventikos (1998). Here it suffices to mention that we solve them in generalized, curvilinear coordinates using a finite-volume approach that is second-order accurate both in space and time. All results presented herein were obtained on a mesh with $153 \times 97 \times 97$ grid nodes in the axial and transverse direction, respectively (see Sotiropoulos & Ventikos 2001 for the details of the mesh topology). Systematic grid refinement studies showed that this grid density is sufficient for resolving both the Eulerian and Lagrangian characteristics of the flow (see discussion in § 3).

Given a steady-state Eulerian flow field, calculated with the numerical method described above, solution of the Lagrangian transport problem requires the temporal integration of the equations for the passive advection of particles in three dimensions:

$$\frac{\mathrm{d}x}{\mathrm{d}t} = u(x, y, z), \quad \frac{\mathrm{d}y}{\mathrm{d}t} = v(x, y, z), \quad \frac{\mathrm{d}z}{\mathrm{d}t} = w(x, y, z). \tag{2.1}$$

The above equations comprise a finite-dimensional dynamical system, which for appropriate velocity fields could exhibit very complex chaotic dynamics (Aref 1984). In this work, equations (2.1) are integrated in time using a fourth-order-accurate, Runge–Kutta method (see Buchanan & Turner 1992 for details) along with a tri-linear scheme for spatial interpolation. To ensure that the chaotic dynamics we uncover herein are real flow features and not artifacts of the specific numerical scheme, we carried out extensive numerical sensitivity studies by: (i) varying the size of the time-increment, Δt; and (ii) implementing and evaluating the accuracy of various spatial interpolation algorithms. Time-step-insensitive Lagrangian dynamics were obtained for $\Delta t \leqslant 10^{-3}$, and thus all subsequently presented results have been been obtained with $\Delta t = 10^{-3}$. It is important to note that using sufficiently small time-increment was found to be essential for the accurate resolution of important features of the Poincaré maps presented in § 6 below – for a volume-preserving system,

large time-increments typically result in non-physical spiralling of orbits on stable surfaces and fail to capture leaky barriers to transport, such as cantori. The spatial interpolation scheme was also found to be of critical importance for resolving the complex features of the velocity field, especially near critical points in the flow, and is discussed in some detail in the next paragraph.

Straightforward spatial interpolation procedures, based on simple averaging or weighted averaging (the so-called inverse distance method), were found inadequate as they failed to resolve trajectories near the spiral-out and spiral-in saddles at the upstream and downstream ends of the vortex breakdown bubble. Similar inadequacies were found when using three consecutive linear interpolation steps, where linear interpolation takes place sequentially between the three pairs of opposite cell faces that comprise a computational cell. The scheme that proved adequate for resolving the complex structure of the velocity field is a tri-linear interpolation scheme in the physical domain, which is as follows (see Murman & Powell 1989 for the two-dimensional analogue of this procedure):

$$u(x, y, z) = A_1xyz + A_2xy + A_3xz + yzA_4 + xA_5 + yA_6 + zA_7 + A_8. \qquad (2.2)$$

The coefficients A_i are computed by solving an 8×8 linear system of equations that is formed when each of the eight nodal points of the cell is used to cast a similar equation. A higher accuracy scheme of this form based on tri-cubic interpolation was also tested. In this case, three mesh cells in each spatial direction (instead of a single cell for the tri-linear case) are involved in the approximation, which leads to a 4^3-term equation and requires the inversion of a 64×64 linear system. Provided that all other numerical parameters are kept the same, tri-linear and tri-cubic interpolation were found to yield practically identical trajectories. Since the computational overhead for the tri-cubic interpolation is significantly higher, the tri-linear approach has been employed to obtain all subsequently presented results.

As an additional accuracy check of our particle-integration algorithm, we compared Poincaré maps (see § 6 below) calculated with our scheme with those obtained using a commercially available graphics and visualization software package – the particle integration module of Tecplot ® Version 8.0 was used for this purpose. Both codes yielded identical results.

3. Overview of the computations and comparisons with experiments

We have carried out time-accurate, three-dimensional computations for two container aspect ratios ($H/R = 1.75$ and 2.0) and for various Reynolds numbers in the steady and unsteady flow regimes. Extensive comparisons of the computed solutions with the experimental findings of Spohn *et al.* (1998) have been presented in Sotiropoulos & Ventikos (2001). Our numerical simulations captured every aspect of the laboratory flow with remarkable accuracy. A small sample of the comparisons between our calculations and the laboratory observations is shown in figure 3, which depicts numerically (Sotiropoulos & Ventikos 2001) and experimentally (Spohn *et al.* 1998) obtained visualization images of the steady vortex breakdown bubble for $Re = 1850$ and $H/R = 1.75$. Both images reveal that there is a toroidal region in the interior of the bubble that remains relatively free of visualization markers (see § 6 for a detailed discussion of this region's complex dynamics) and that the downstream end of the bubble is characterized by the presence of distinct asymmetric folds. Notice in particular the excellent agreement between the computed and observed shapes of these folds (we clarify their origin in § 4). Furthermore, in the wake of both the

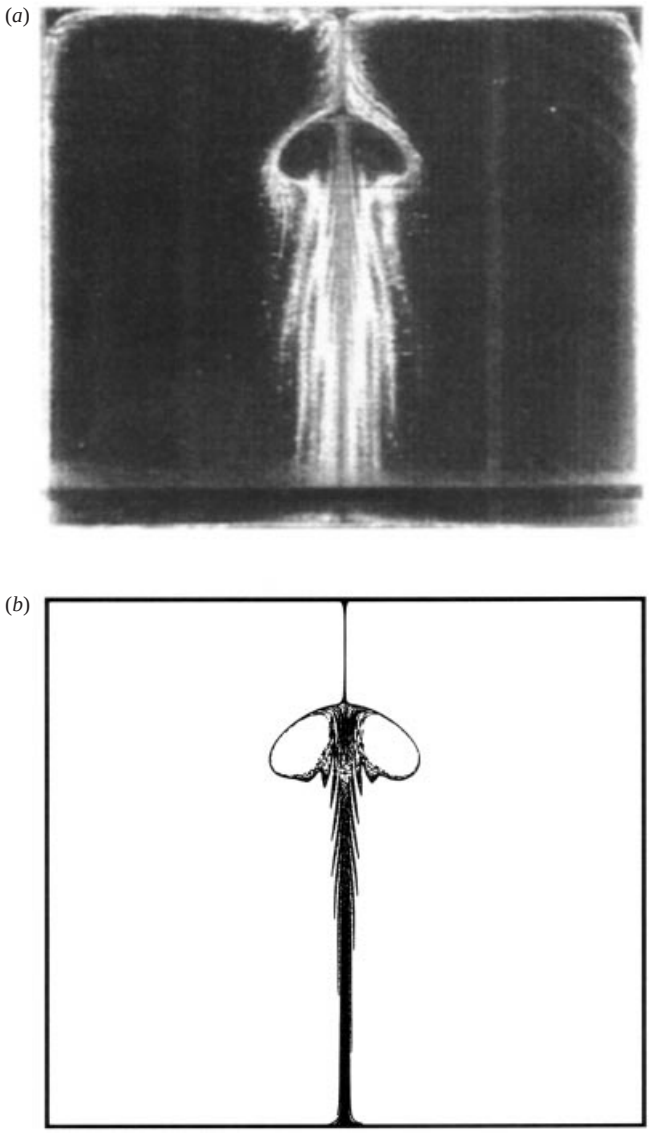

FIGURE 3. Experimental (*a*) and calculated (*b*) images of a steady vortex breakdown bubble for $Re = 1850$ and $H/R = 1.75$. (*a*) Flow visualization with electrolytic powder particles released from a solder wire on the cylinder wall. Reproduced with permission from Spohn *et al.* (1998). (*b*) The calculated image was constructed by releasing particles from equally spaced points along concentric circles located just below the stationary cover. The radius of the outermost circle is $0.004R$.

computed and observed breakdown bubbles the markers are organized in a series of short straight clusterings, which form a non-axisymmetric, staggered about the axis, arrangement.

The above comparisons establish the accuracy of both the flow solver and the trajectory- integrator techniques we employ for constructing the Lagrangian images (for more extensive comparisons see Sotiropoulos & Ventikos 2001). Achieving such a level of agreement with the laboratory visualizations, allows us to proceed confidently with the Lagrangian interrogation of the Eulerian flow fields. Before we do so,

however, we should comment on some important numerical difficulties we had to overcome before we could obtain the level of agreement indicated by the comparisons in figure 3.

As we discuss in Sotiropoulos & Ventikos (2001), we carried out extensive mesh sensitivity studies using a series of successively finer computational meshes. Flowfields obtained on grids not sufficiently refined in the vicinity of the bubble – for the purpose of our discussion we shall refer to such grids as 'coarse' grids – were found to exhibit erroneous Lagrangian dynamics within the breakdown region. Particles that enter the vortex breakdown bubble, through its downstream end, were found to get trapped 'indefinitely' in its interior. To clarify the term 'indefinitely', we should point out that we continued the integration of the particle trajectories for very long times and with a variety of time increments without the particles ever escaping. The computed trajectories were found to densely cover almost the entire space in the interior of the bubble before getting attracted onto a slender torus from which they never escaped. That is, the experimentally observed tracer-free toroidal region in the interior of the bubble (see figure 3), which as we will subsequently show exhibits very rich Lagrangian dynamics, could not be reproduced on such grids. To eliminate this numerical artifact, we employed computational meshes that were carefully refined within the inner toroidal region of the breakdown bubble. Even though such grid refinement did not significantly alter the velocity field (differences between coarse and fine mesh predictions nowhere exceeded 3% to 5%), it had a profound effect on the Lagrangian dynamics. As we will subsequently show, the velocity fields obtained on the refined grids yield particle trajectories that are extremely sensitive to initial conditions. Particles originating from arbitrarily close initial locations (where 'arbitrarily close' is determined by the precision of the arithmetic we employ in our computer calculations) diverge exponentially in time as they re-circulate within the vortex breakdown region (see figure 4 for typical particle trajectories in the interior of the bubble). This very important feature, which establishes the chaotic dynamics of the flow, cannot be captured on the coarse meshes in which initially nearby particles were found to remain close at all times.

4. Three-dimensional flow topology and the Šil'nikov mechanism

To facilitate our discussion in this section, we begin by illustrating typical particle paths within the vortex breakdown region. Subsequently we discuss the three-dimensional structure of the invariant manifolds of vortex breakdown bubbles. We consider the topology of both ideal (axisymmetric) and real-life (observed in the laboratory and calculated herein on curvilinear meshes) flow fields. Since the latter can be interpreted as the result of superimposing stationary, non-axisymmetric disturbances on the former, the juxtaposition of these two cases will help us clarify the manner in which three-dimensional modes alter the dynamics of the ideal flow field. We analyse the topological features of vortex breakdown flows in tandem with those of a rather simple autonomous, three-dimensional dynamical system, which has been previously studied by Broer & Vegter (1984) (see also Wiggins 1990). We find the phase-space dynamics of this system to be essentially identical to the physical-space dynamics of stationary vortex breakdown bubbles. The similarities between the two systems point to a specific chaos-inducing mechanism in real-life vortex breakdown flow fields.

Figure 4 shows calculated trajectories of three particles, each selected to illustrate various aspects of the three-dimensional flow field. The 'thick' orbit, which is representative of upstream originating orbits that never visit the breakdown region, is deflected

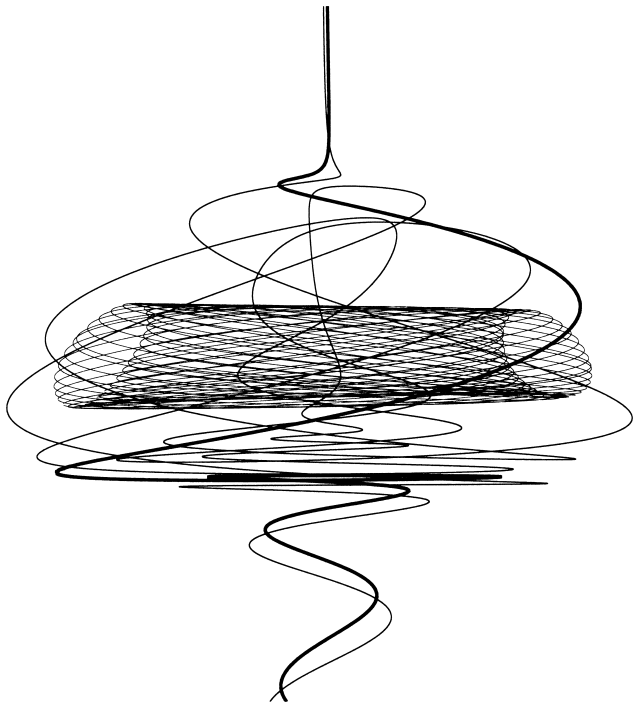

FIGURE 4. Calculated typical three-dimensional particle trajectories in and around the breakdown bubble ($Re = 1850$, $H/R = 1.75$). The 'thick' orbit is released from the axis upstream of the breakdown bubble. The 'thin' orbit is released just off the axis also upstream of the bubble. The toroidal orbit is released within the interior region that remains free of markers in figure 3.

off the axis and begins to spiral around it, spanning the outer portion of a bubble-like structure. At the downstream end of the bubble, the orbit converges radially inward, spirals around the downstream stagnation point (the precise topological nature of both the upstream and downstream stagnation points will be clarified below) and continues its downstream spiralling motion confined in the immediate vicinity of the axis. The 'thin' orbit in figure 4 is representative of upstream originating orbits that enter the vortex breakdown bubble. Its initial path is similar to that of the 'thick' orbit until the downstream stagnation point is approached, where it reverses direction, enters the bubble, and begins to spiral toward the upstream stagnation point. When it reaches there, it begins to diverge away from the axis, spiralling along the interior of the bubble-like surface. Subsequently, the orbit passes again through the downstream stagnation point where it may either exit to continue downstream or (as shown in figure 4) repeat the same cycle of motion for arbitrarily many times (see § 7 and § 8) before it finally exits. The toroidal orbit in figure 4 is representative of orbits confined in the interior of the bubble, that is the region that remains clear of particles in figure 3. Such orbits appear to move along two-tori (see § 6). We should caution that we imply no general connection between the particle release location in figure 4 and its subsequent fate. The relation between initial conditions and residence time within the breakdown bubble is very complex and is discussed in detail in § 7.

Let us now consider the manifold structure of an axisymmetric, or ideal, stationary vortex breakdown bubble (see Holmes 1984; Wiggins 1990; MacKay 1994). Figure 5(*a*) shows a sketch of the diametral cross-section and the three-dimensional structure of

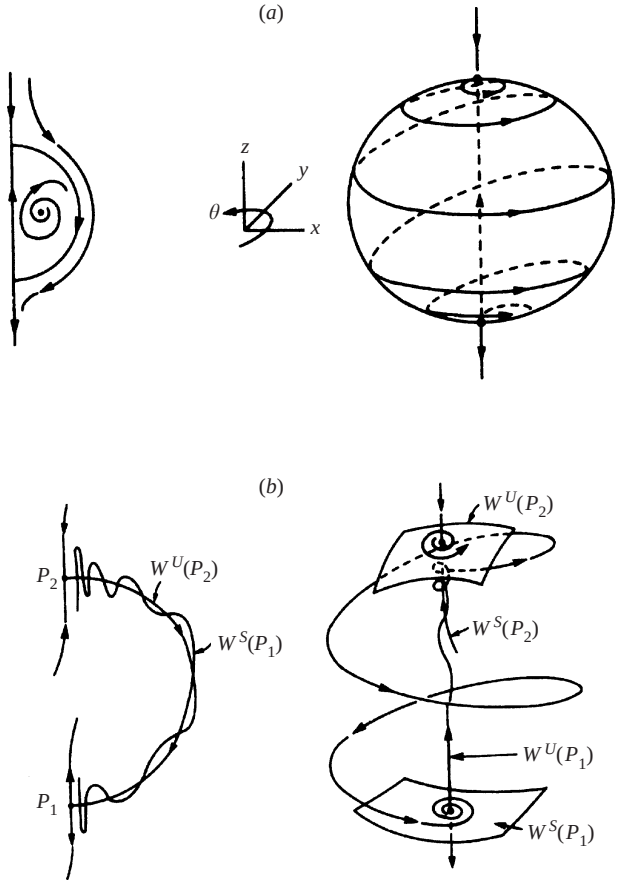

FIGURE 5. (*a*) Cross-section and three-dimensional structure of the heteroclinic cycle for the truncated normal form, equation (4.1); and (*b*) cross-section of the perturbed manifolds and homoclinic orbits for the full normal form (including the effect of higher order terms). Taken from Wiggins (1990).

the heteroclinic cycle for the three-dimensional, axisymmetric flow field. There are two saddle-type fixed hyperbolic points (or stagnation points) along the container axis, which we denote as P_1 and P_2, respectively. The two-dimensional unstable manifold $W^U(P_2)$ and one-dimensional stable manifold $W^S(P_2)$ of P_2 coincide with the two-dimensional stable manifold $W^S(P_1)$ and one-dimensional unstable manifold $W^U(P_1)$ of P_1. Consequently, the resulting heteroclinic cycle creates an invariant bubble-like surface, which delineates the interior recirculating flow from the outer flow as shown in figure 5(*a*). Outside fluid cannot penetrate the interior of the bubble, which is occupied by trapped fluid that moves along invariant two-tori, the streamsurfaces of the axisymmetric flow – see Mezić & Wiggins (1994) and Haller & Mezić (1998) for a detailed discussion on the existence of a streamfunction in axisymmetric flows.

The previously described axisymmetric topology is identical to the phase-space dynamics of the following autonomous three-dimensional normal form (Wiggins 1990):

$$\frac{\mathrm{d}r}{\mathrm{d}t} = \mu_1 r + arz + \cdots, \quad \frac{\mathrm{d}z}{\mathrm{d}t} = \mu + 2 + br^2 - z^2 + \cdots, \quad \frac{\mathrm{d}\theta}{\mathrm{d}t} = \omega + \cdots, \tag{4.1}$$

where μ_1, μ_2, a, b, f, and ω are constants, and the dots imply higher-order terms. As shown in Wiggins (1990), for $a > 0$ and $b = -1$ the stable and unstable manifolds

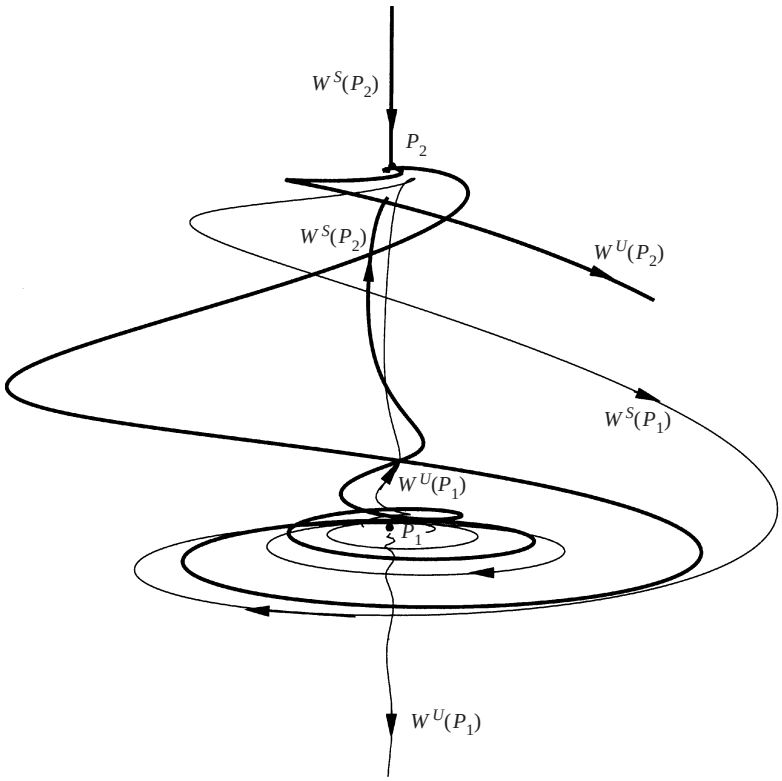

FIGURE 6. Three-dimensional orbits representative of the stable and unstable manifolds of the fixed hyperbolic points for a calculated vortex breakdown bubble ($Re = 1850$, $H/R = 1.75$).

of the hyperbolic fixed points of this system create an invariant sphere, similar to that shown in figure 5(*a*), and the periodic orbits become invariant two-tori. The axisymmetric dynamics of this system can be radically altered by the addition of higher-order terms in the right-hand side of (4.1). Including such terms, no matter how small they may be, destroys the symmetry of the basic form and breaks the invariant structure of the sphere shown in figure 5(*a*) (Broer & Vegter 1984; Wiggins 1990). More specifically, the one-dimensional unstable manifold of P_1 and the one-dimensional stable manifold of P_2 will no longer intersect in three-dimensional space. Moreover, we would also anticipate the two-dimensional manifolds of P_1 and P_2, $W^S(P_1)$ and $W^U(P_2)$ to intersect transversely along heteroclinic orbits (see sketch in figure 5*b*) – this is a consequence of a version of the Kupka–Smale theorem for volume preserving systems (see Broer & Vegter 1984). It is, therefore, possible for the portion of $W^U(P_1)$ ($W^S(P_2)$) inside the bubble to fall into $W^S(P_1)$ ($W^U(P_2)$) forming homoclinic orbits in three-dimensional space (Broer & Vegter 1984; Wiggins 1990) – that is, infinite period orbits which are doubly asymptotic to a fixed point of saddle type as $t \to \pm\infty$.

We now argue that similar topological features also mark the differences between ideal and real-life vortex breakdown flow fields. Figure 6 depicts calculated three-dimensional trajectories representative of the stable and unstable manifolds of the fixed hyperbolic points for a stationary vortex breakdown bubble. The destruction of the one-dimensional on-axis saddle-to-saddle connection is clearly evident in this figure. Moreover, figures 4 and 6 demonstrate that both the upstream and downstream

fixed hyperbolic points of a real-life vortex breakdown bubble are of saddle-focus type – that is, fixed points at which the velocity gradient tensor has one real and two complex eigenvalues. Adopting the terminology introduced in Jackson (1991), we shall refer to the P_1 and P_2 points as spiral-in and spiral-out saddles, respectively – the three-dimensional structure of orbits near these two points is further clarified in figure 7. The trajectories shown in figure 6 approximate the general structure of orbits homoclinic to the two saddles. It is, of course, very difficult to compute an exact homoclinic orbit as an arbitrarily large number of time steps may be required to complete the homoclinic connection (see discussion in § 5). Nevertheless, the calculated trajectories in figure 6 are remarkably similar to the homoclinic orbits resulting when higher-order terms are included in the right-hand side of (4.1), as these have been envisaged and sketched by Wiggins (1990) (see figure 5*b*). We should also point out that the above topological features of a real-life vortex breakdown bubble are identical to those of a perturbed spheromak, or spherical vortex (MacKay 1994). The spheromak is an axisymmetric magnetic field configuration (proposed as a means for confining plasma in nuclear fusion reactors) whose manifold structure is identical to that depicted in figure 5 – MacKay (1994) also points out the relevance of the spherical vortex to the bubble-type mode of vortex breakdown. In discussing the effects of mild perturbations on the integrable axisymmetric form, MacKay (1994) describes essentially the manifold structure shown in figures 4 and 6. MacKay (1994) puts forth a number of important ideas concerning the dynamics of a perturbed spheromak, many of which are confirmed by our findings, and for that reason we shall revisit this very insightful contribution in subsequent sections of this paper.

It is well established from the theory of dynamical systems that homoclinic orbits are structurally unstable and their occurrence signals the onset of chaotic dynamics (Arneodo, Coullet & Tresser 1982; Gaspard & Nicolis 1983). The importance of such orbits was first recognized by Šil'nikov (1965) who proved that homoclinic orbits, mapping a saddle-focus fixed point to itself, possess a countable infinity of Smale horseshoes. Since our computations (see figures 4, 6, and 7) have established that the two fixed hyperbolic points defining a vortex breakdown bubble are indeed of saddle-focus type, we argue that the so-called Šil'nikov mechanism is responsible for: (i) the destruction of the invariant axisymmetric bubble surface; and (ii) the chaotic stirring of particles that enter the bubble and pass repeatedly through the two saddle foci before they exit. The pivotal role of the spiral-in and spiral-out saddles in stretching and folding material elements (thus, causing the formation of a countable infinity of horseshoes) will be illustrated in § 5. Notice, however, that even a simple inspection of the very complex structure of the stable and unstable manifolds of P_1 and P_2 shown in figure 7 strongly suggests that such chaos-inducing phenomena will occur.

Our conjecture concerning the role of Šil'nikov's mechanism is further supported by the work of Broer & Vegter (1984). As we have discussed above, they studied the effects of higher-order terms in (4.1) and proved that for the perturbed system a sequence of Šil'nikov's bifurcations will occur, leading to the formation of a countable infinity of Smale horseshoes and non-integrable dynamics. Figure 8, from Broer & Vegter (1984), shows their interpretation of the three-dimensional structure of the stable and unstable manifolds of the two saddle foci for a perturbed, volume-preserving system of the type described by (4.1). Notice the striking similarity between the asymmetric folds in the vicinity of the 'north pole' in this sketch and those observed in the laboratory and calculated herein (figures 3 and 7) near the spiral-in saddle of stationary vortex breakdown bubbles. As pointed out by Wiggins (1990), the three-dimensional perturbations that need to be superimposed on equations (4.1) to

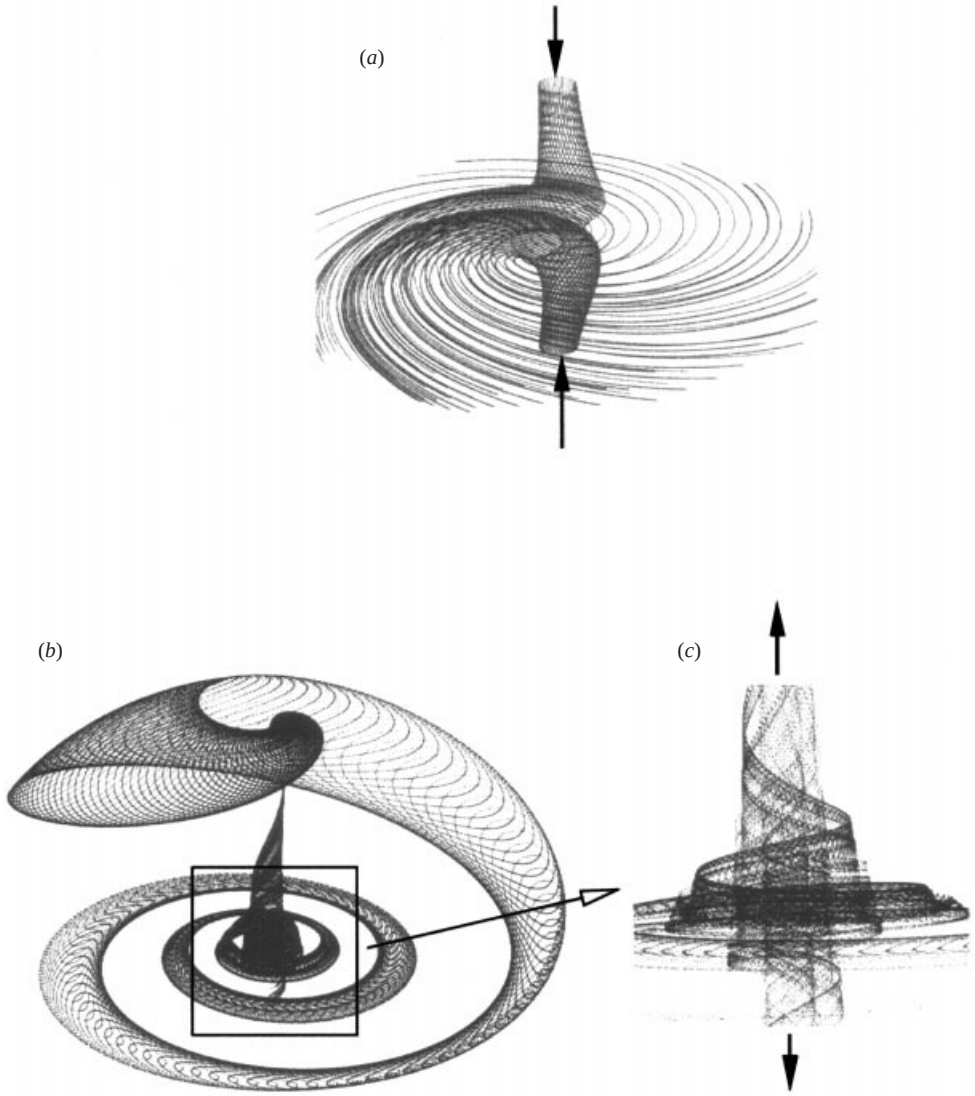

FIGURE 7. Three-dimensional topology of orbits in the vicinity of the spiral-in and spiral-out saddles. (*a*) Orbits near the spiral-out saddle (P_2) are visualized by releasing particles from two circles (centered about the axis) located above (outside the bubble) and below (inside the bubble) P_2. The initial conditions are axisymmetric. The one-sided, spiral-like deflection of the two sets of orbits, as they 'collide' at P_2, is indicative of the spiral-out nature of the upstream fixed hyperbolic point of the bubble. (*b*) Orbits near P_2. A material circle (centred about the axis) is introduced just above P_2 and a sequence of instantaneous snapshots, as it spirals toward P_1 and gets stretched by the flow, are superimposed. Notice how the material circle is captured by the two-dimensional stable manifold of P_1 and the particles that comprise it split between the upward (entering the bubble) and downward directed unstable manifolds of P_1. (*c*) Magnified view of (*b*) near P_1, illustrating the spiral-in saddle nature of the downstream fixed hyperbolic point.

alter the topology from that shown in figure 5(*a*) to that depicted in figure 8 are exponentially small. This is a very important point as it suggests that it may be very difficult to produce in the laboratory axisymmetric vortex breakdown bubbles, as that would require eliminating from the experimental rig practically every disturbance no matter how small it is.

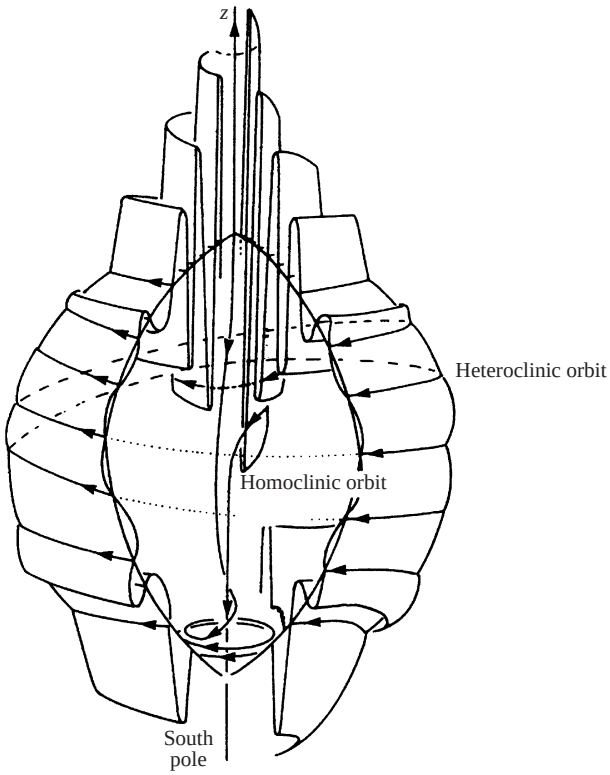

FIGURE 8. Cut-open perturbed globe showing a Šil'nikov homoclinic orbit for a volume-preserving system. Taken from Broer & Vegter (1984).

An important parameter in theoretical studies of Šil'nikov-type bifurcations (Šil'nikov 1965; Glendinning & Sparrow 1986; Broomhead & King 1986; Mullin 1993) is the ratio of eigenvalues of the saddle foci. As we discussed above, at a saddle focus the velocity gradient tensor has one real and two complex eigenvalues λ and $\rho \pm \mathrm{i}\omega$, respectively, with $\lambda, \rho, \omega > 0$ and real. The relevant eigenvalue ratio is defined as $\delta = \rho/\lambda$ and can be interpreted as the ratio of the speed of rotation along the spiralling two-dimensional manifold of the saddle focus to the ejection speed along its corresponding one-dimensional manifold (Mullin 1993). Glendinning & Sparrow (1986) showed that the dynamics near a saddle focus, and in particular the emergence of infinite-period homoclinic orbits as a control parameter is varied, depend critically on δ (see also Mullin 1993), with very complex Šil'nikov-type dynamics expected to occur when $\delta < 1$. Experimental verification of this theory has been reported by Healey *et al.* (1991) who studied the phase-space dynamics of a modified Van der Pol oscillator (see also Mullin 1993). It should be pointed out, however, that these results have been obtained for dissipative dynamical systems. For the present volume-preserving case the incompressibility of the velocity field along with the fact that the sum of the eigenvalues of the velocity gradient tensor is equal to its trace, i.e. the divergence of the velocity field, imply that δ is always equal to 0.5 at a saddle focus. Interestingly, therefore, and even though the condition for Šil'nikov dynamics to occur is always satisfied at a saddle focus in an incompressible flow, the dynamical bifurcations of three-dimensional, volume-preserving systems are insensitive to the ratio of eigenvalues.

Finally, we should mention that phase-space Šil'nikov dynamics in fluid flow problems have been previously uncovered experimentally (by reconstructing phase portraits from time-series measurements) in Taylor–Couette flows (Mullin & Price 1989) and more recently in nematic liquid crystal flows (Peacock, Mullin & Binks 1999). To the best of our knowledge, however, the vortex breakdown flow fields studied herein are the first experimentally realizable and numerically reproducible flows in which the onset of chaotic dynamics in physical space can be interpreted in terms of Šil'nikov's theorem. In an earlier study, Holm & Kimura (1991) studied the Lagrangian kinematics of the Chandrashekar flow, an analytical flow derived from the linearized Rayleigh–Bénard convection equations, which exhibits a spatially periodic heteroclinic network of saddle-focus connections. They argued that small perturbations induced by their numerical integration scheme, amplified when passing repeatedly through the network of spiral foci, could eventually lead to the onset of Šil'nikov chaos. Their conjecture, however, could not be rigorously established by their computations as the numerical integrator they employed did not produce sensitive dependence on initial conditions (Holm & Kimura 1991). In the following sections we establish numerically the onset of chaotic dynamics within stationary vortex breakdown bubbles, thus documenting the first application of Šil'nikov's theorem to the physical space of a real-life flow field.

5. Stretching, folding, and chaotic stirring

Our conjecture in the previous section, concerning the role of Šil'nikov's mechanism in inducing chaotic dynamics, is based on the assumption that homoclinic orbits, mapping the saddle foci to themselves, do exist. It is important to emphasize, however, that a rigorous proof of this critical prerequisite for Šil'nikov's theorem to be valid is very difficult, if not impossible, for a general nonlinear dynamical system (see related discussion in Broomhead & King 1986). In fact, even for analytically prescribed velocity fields the existence of homoclinic orbits can be rigorously established only on a case-specific basis by selecting simple analytical functions (Arneodo *et al.* 1982). Rather than attempting, therefore, to prove that homoclinic orbits exist in vortex breakdown velocity fields, we demonstrate herein the consequences of their existence: the formation of infinitely many Smale horseshoes in the vicinity of the saddle foci and the resulting efficient stirring of Lagrangian markers.

To demonstrate the formation of horseshoes and the resulting sensitive dependence on initial conditions, we plot in figure 9 the evolution of a material line as it recirculates within the breakdown bubble. The element consists of 1000 particles initially arranged to form a straight line. Each particle is identified by a number, based on its initial ordering along the line element, so that the deformation of the element can be monitored at subsequent times. The initial length of the element is $10^{-5}R$ and, thus, the initial distance between neighbouring particles is $10^{-8}R$. The element originates just upstream of the breakdown bubble in the vicinity of the axis. It enters the breakdown region through the spiral-in saddle and recirculates within the bubble several times before all particles that comprise it exit. The shapes of the element at six successive instants in time are shown in figure 9 while the temporal growth of its total length is plotted in figure 10. The element position at each of the time instants we monitor is marked with numbers in figure 9. Position 1 is the initial release location while position 2 is just prior to the element passing through the spiral-in saddle for the first time. Positions 3, 4, and 5 are snapshots during the second approach of the element toward the spiral-in saddle (the element has already

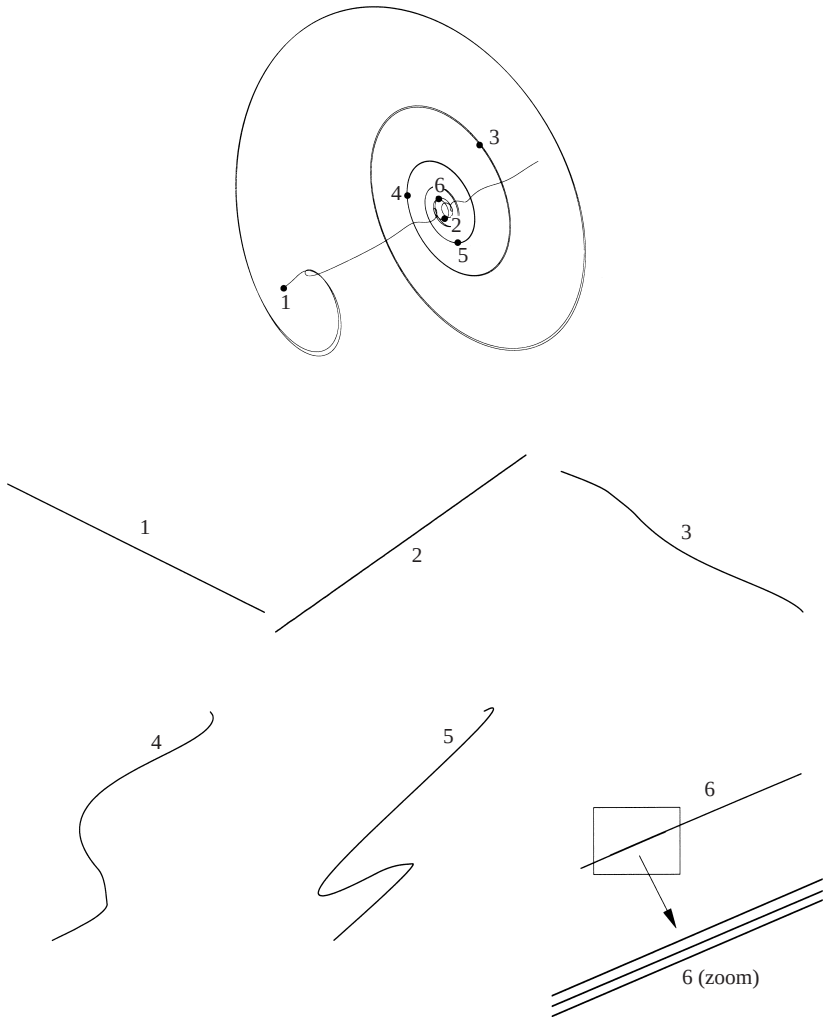

FIGURE 9. Evolution of the shape of an initially straight material line as it recirculates within a stationary vortex breakdown bubble ($Re = 1850$, $H/R = 1.75$). The material filament consists of 1000 particles spaced uniformly $10^{-8}R$ apart (the initial length of the filament is $10^{-5}R$). The various positions of the filament during its motion within the breakdown region are marked with numbers along the trajectory of its midpoint. The element shape at every location is shown at an appropriately enlarged scale for clarity.

recirculated once within the bubble). Finally, position 6 is just before the element enters the breakdown region for the third time.

As the element begins to spiral initially away from the axis and subsequently inward, toward the spiral-in saddle (location 1 to 2), its length (see figure 10) starts growing but without any visible increase in its curvature. The first passage through the spiral-in and spiral-out saddles, however, has a dramatic effect on both length and curvature. As seen in figure 10, the growth rate of element length undergoes a steep increase as soon as it passes through the spiral-in saddle for the first time (i.e. from location 2 to 3). Furthermore, at position 3 the initially straight element has already become wavy and its curvature continues to grow rapidly as it spirals inward toward the spiral-in saddle for the second time (from 3 to 5). In fact the intense and

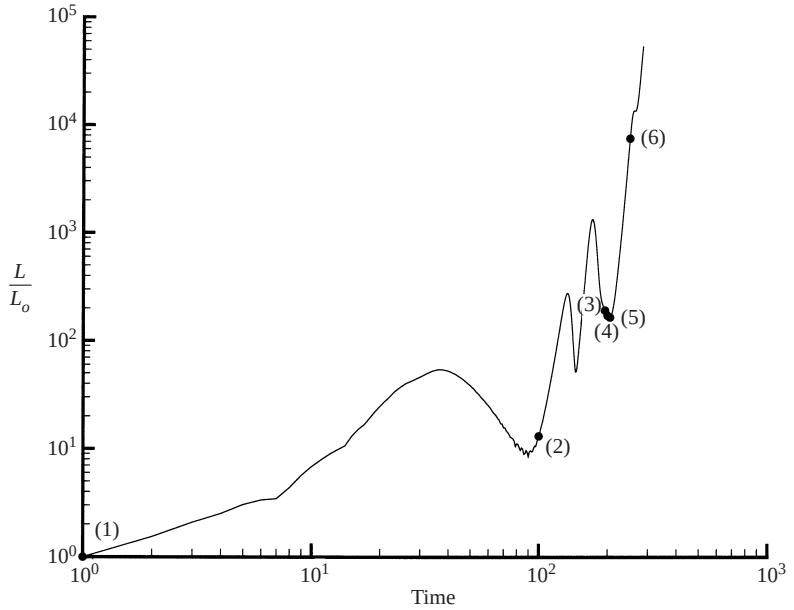

FIGURE 10. Temporal evolution of the length of the filament shown in figure 9. The numbers in this figure indicate the various positions of the element defined in figure 9. The length (L) has been scaled by the initial length (L_o). The rotating lid completes one revolution in π time units.

very rapid folding of the element between positions 3 to 5 is a clear indication that Šil'nikov's mechanism, the formation of infinitely many Smale horseshoes, is indeed at work in the vicinity of the saddle focus. At location 6, as the element approaches the spiral-in saddle for the third time, fine-scale striations have formed that can be made visible only by zooming into smaller spatial scales. Moreover, the element's length has increased by approximately four orders of magnitude from its initial length. The exponential growth of length and curvature within the breakdown region demonstrates the extreme sensitivity to initial conditions, establishes the existence of at least one positive Liapunov exponent and proves conclusively the chaotic dynamics of the calculated vortex breakdown flow fields.

To explore the chaotic stirring of passive Lagrangian markers by a stationary vortex breakdown flow field, we show in figure 11 the calculated temporal evolution of a series of initially circular material elements. The elements are arranged along a hemispherical surface at the upstream face of the bubble and individual particles are coloured according to their axial position (figure 11*a*). The stretching and folding of material lines near the two saddles are clearly evident in figures 11(*c*) to 11(*f*), which span a time interval during which the material lines have passed through the spiral-in saddle. As the markers continue to re-circulate, the initial structure of the circular filaments disappears rather rapidly and eventually well-stirred, chaotic regions are evident almost everywhere within the bubble. As seen in figure 11(*i*), however, even after several iterates of the chaotic map – the elapsed time since the start of this numerical experiment corresponds to approximately 150 revolutions of the rotating lid – there are coherent single-colour filaments still visible throughout the bubble. The presence of such filaments appears to indicate the existence of regions of inefficient stirring within the breakdown region and suggests an important area that deserves further study, namely the rigorous quantification of the intensity of chaotic

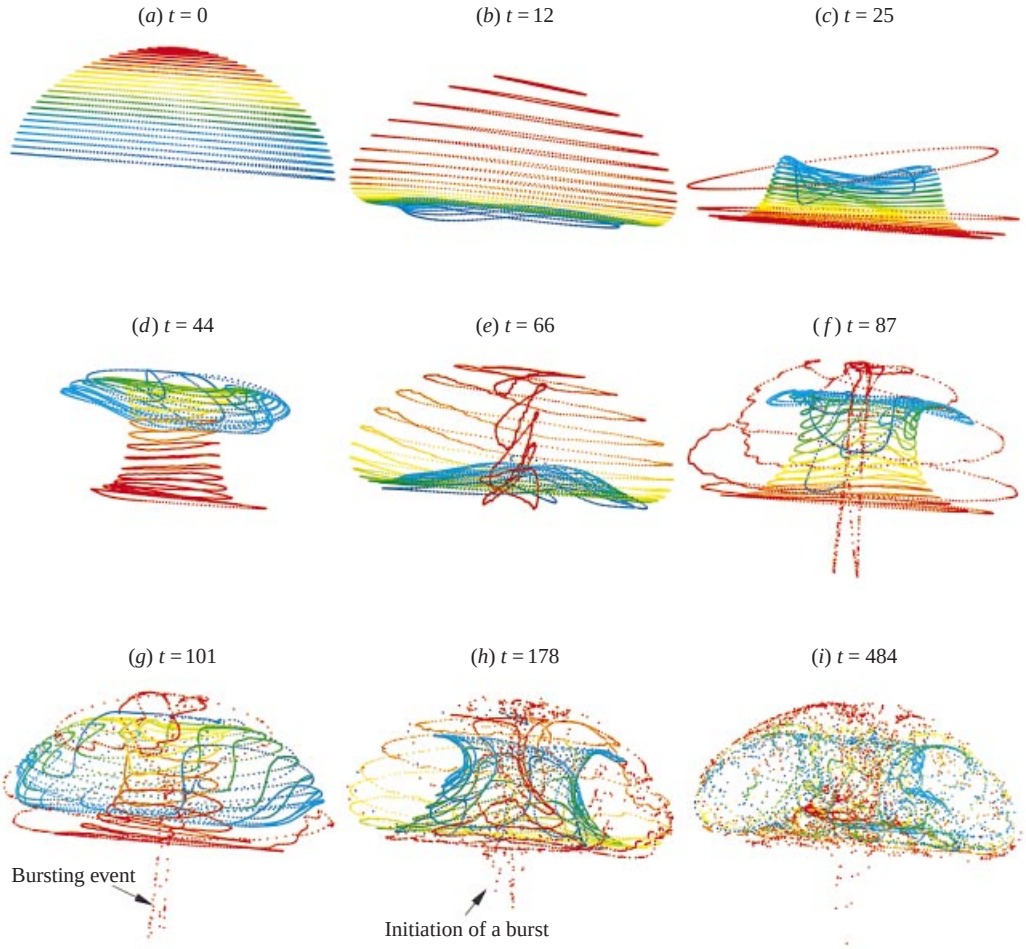

FIGURE 11. Temporal evolution of series of circular material lines, initially placed to span the upstream face of the vortex breakdown bubble ($Re = 1850$, $H/R = 1.75$). Individual particles are coloured based on their axial coordinate at $t = 0$. A total of 10 000 particles have been used in this simulation. The rotating lid completes one revolution in π time units.

stirring for varying Reynolds numbers and container aspect ratios. We are currently conducting such studies, by calculating Liapunov exponents and stirring efficiencies, and will report their results in a future communication.

An animation video we have created using the complete sequence of images such as those shown in figure 11 sheds new light on the emptying process of the breakdown bubble. More specifically, we find that the markers do not exit the bubble in a continuous fashion, but rather in a sequence of distinct bursting events during which clusters of markers exit the bubble simultaneously. Typical bursting events are clearly evident in figures 11(f) to 11(i). Figures 11(f) and 11(g), for instance, depict bursting events well under way while figure 11(h) shows such an event during its early stages. The number of particles that exit during a given burst is not always the same but appears to vary in a random manner – compare, for instance, figures 11(g) and 11(i). Similar seemingly random variations appear to characterize the distribution of the waiting times between successive bursts. The reason for this complex behaviour is

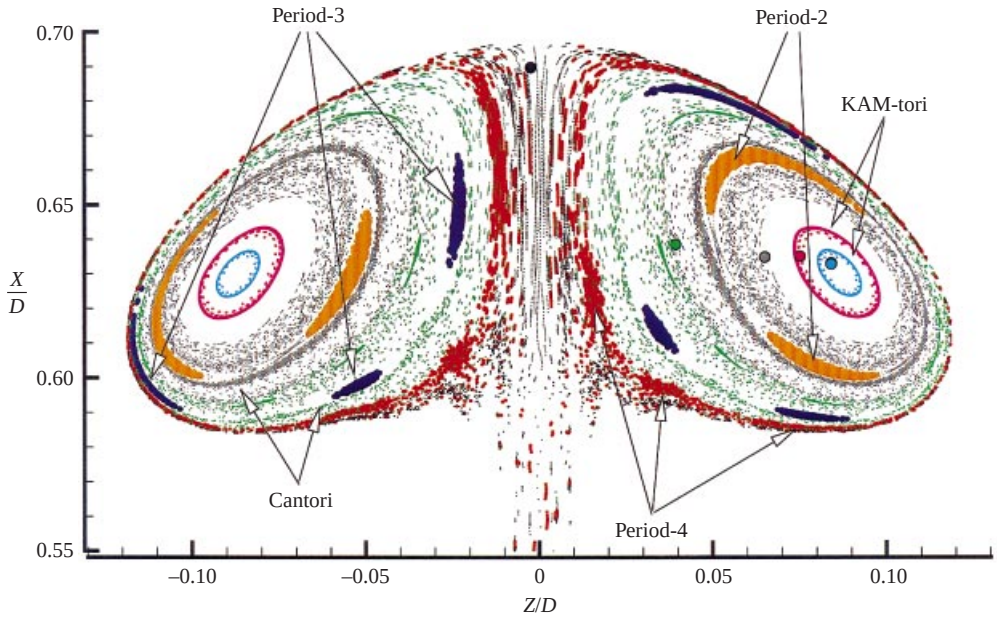

FIGURE 12. Poincaré section of the steady vortex breakdown bubble for ($Re = 1850$, $H/R = 1.75$). Same-colour blobs of markers (5 markers per colour) were released along short straight segments, selectively placed within various regions in the interior of the breakdown bubble to elucidate the richness of the dynamics. The large dots mark the initial locations of the various blobs (dots are shown only for those blobs that were not placed within unmixed islands). Each orbit has been iterated for 10^6 time steps. The surface of section is a diametral slice of thickness $0.01R$.

explained in § 7 and § 8 where we explore the fractal properties of particle residence-time maps.

Finally, we should caution that figure 11(*i*) may convey the false impression that markers have spread throughout the entire breakdown region. The toroidal region in the interior of the bubble, however, remains relatively free of upstream originating markers. In the following section we construct three-dimensional maps and Poincaré sections for a variety of initial conditions to clarify the dynamics of this toroidal region.

6. Poincaré sections

In this section we analyse the Lagrangian dynamics in the interior of stationary vortex breakdown bubbles. We construct three-dimensional maps by calculating the trajectories of several initial conditions over long time intervals. To visualize such a map, we define a diametral slice of given thickness and mark all intersections of the three-dimensional orbits with this slice. The resulting two-dimensional map is a Poincaré section. To facilitate the interpretation of the results, all markers that originated from the same set of initial conditions are the same colour.

Figure 12 depicts the Poincaré section for the steady vortex breakdown bubble shown in figure 3. The previously discussed Šil'nikov mechanism is responsible for the formation of the stochastic, columnar filament (black orbits) in the vicinity of the axis. Recall that within this filament, chaotic orbits spiral upward around the axis, from the spiral-in to the spiral out saddle, and then downward again along the inside of the outer surface of the bubble – we shall refer to such orbits as Šil'nikov orbits.

Therefore, the outer surface of the bubble is also occupied by Šil'nikov orbits but due to its very small thickness it is difficult to visualize in a Poincaré section – the chaotic motion of particles along the outer surface of the bubble has already been demonstrated in figure 11.

Šil'nikov orbits recirculate repeatedly within the bubble, wrapping around the toroidal region that remains free of upstream originating markers in figure 3. The Poincaré section in figure 12, however, reveals that this internal region exhibits very rich Lagrangian dynamics. The elliptic point at its centre is surrounded (blue and magenta markers in figure 11) by regular KAM-tori (after Kolmogorov, Arnol'd, and Moser). By definition, a KAM-torus is the invariant locus of quasi-periodic orbits about an elliptic fixed point. Since an orbit starting on an invariant torus remains confined on it, KAM-tori act as impermeable barriers to transport – notice that both the blue- and magenta-coloured markers in figure 12 never escape through their respective KAM-torus. In general, KAM-tori are characteristic of the type of dynamics we would anticipate in the interior of axisymmetric (integrable) stationary vortex breakdown bubbles (see previous discussion in § 4) – for a steady axisymmetric flow KAM-tori coincide with the flow streamlines. In other words, the invariant tori in the core region of three-dimensional vortex breakdown bubbles are the remnants of the integrable axisymmetric dynamics. Their existence is a consequence of the KAM theorem, which shows that many of the simple quasi-periodic solutions of an integrable system will, in general, still be present, virtually unchanged, in a non-integrable system.

It is clearly evident from figure 12, that the similarities between the dynamics of axisymmetric and real-life vortex breakdown bubbles are confined only within the previously discussed core region. The quasi-periodic core is embedded within nested cantori, which, unlike KAM-tori, are only partial barriers to transport. Cantori have a Cantor-set-like structure and act as leaky interfaces (MacKay, Meiss & Percival 1984). The stirring of the grey blob in figure 12 illustrates clearly the dynamics of such partial barriers to transport. Even though these orbits are initially trapped on the grey cantorus, they eventually escape to explore more of the chaotic regime. Yet another cantorus is revealed by the stirring of the green blob. This torus, however, appears to be a considerably leakier barrier than the grey one – notice the relatively few orbits that define it. The gaps between adjacent cantori are populated with chaotic regions as well as un-mixed islands of regular motion. Period-two, -three, -four, and -five islands are clearly visible in figure 12. The complex three-dimensional topology of these unmixed subsets of the flow domain is clarified in figure 13. We should note that other higher-period islands may also exist but their emergence is strongly dependent on the resolution of a given calculation (determined by the number of initial conditions and the total number of iterates we employ). Typically, very high-period islands may require a large number of iterates before they can be clearly distinguished (Ottino 1989).

To illustrate the effects of varying the non-dimensional governing parameters of this flow (Re and H/R) on the dynamics of vortex breakdown bubbles, we show in figure 14 Poincaré sections for two Reynolds numbers, $Re = 1492$ and 1667, for a container with $H/R = 2$. For both bubbles shown in figure 14, the region in the vicinity of the axis is also occupied by the well-stirred Šil'nikov filament discussed above while the interior of the bubble is foliated by quasi-periodic cantori and KAM-tori embedded within stochastic regions. A striking difference between the $Re = 1492$ case and that shown in figure 12 is the apparent lack of any periodic islands in figure 14(a). Even though we searched carefully for initial conditions whose orbits

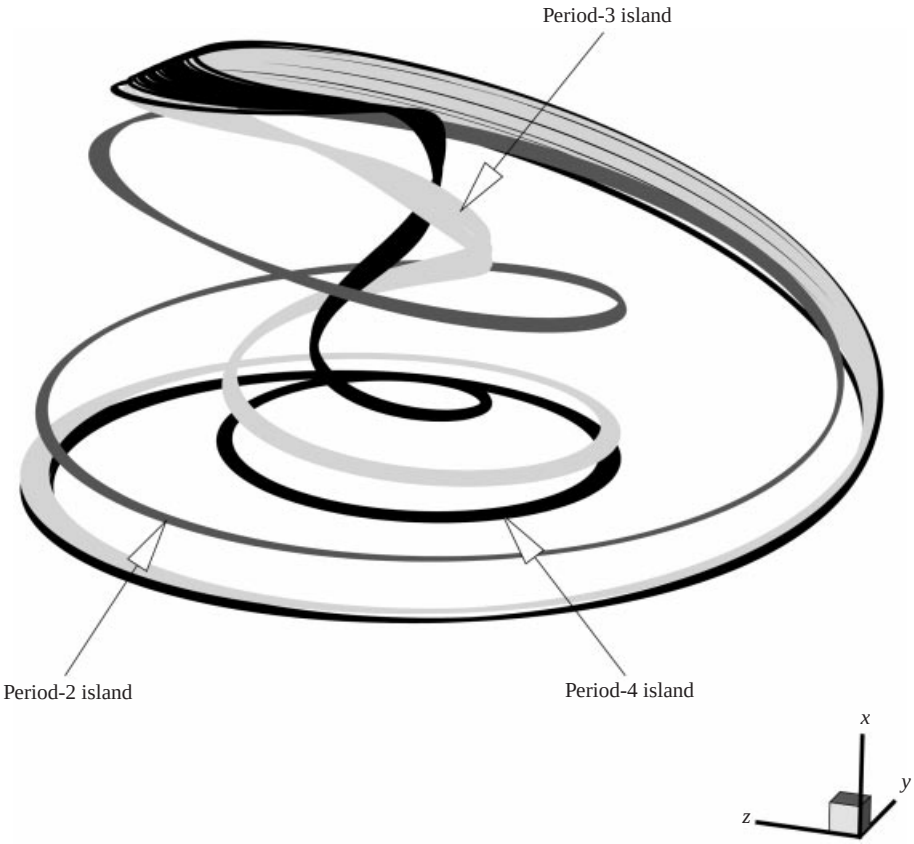

FIGURE 13. Three-dimensional orbits illustrating the intertwining of the period-two, -three, and -four islands in the interior of the bubble shown in figure 12.

remain confined within unmixed islands (similar to those shown in figures 12 and 13), we were not successful in locating any such orbits. We should note, however, that islands of very high period may still be present but, as previously discussed, such long island chains are difficult to visualize. Comparison of the higher Reynolds number case (figure 14*b*) with that shown in figure 14(*a*) reveals that the stochastic columnar filament around the axis has grown in size, the quasi-periodic core has shrunk, and a period-two island has appeared. Impermeable barriers are still present near the core as evidenced by the innermost grey torus. Notice, however, that unlike in the lower *Re* case (figure 14*a*), several orange orbits have exited the bubble, thus suggesting that the inner core tends to become leakier as the Reynolds number increases.

The Poincaré sections shown in figures 12 and 14 serve as a preliminary parametric investigation of the effects of varying governing flow parameters on the chaotic dynamics and transport within vortex breakdown bubbles. Even though the few cases we have included herein are not sufficient to draw definitive conclusions, some important, albeit preliminary, trends emerge. More specifically, our computations reveal that the extend of the chaotic columnar filament in the interior of the bubble as well as the overall structure of the interior toroidal region are both strong functions of *Re* and H/R. Comparing figures 14(*a*) and 14(*b*), for instance, suggests that the size of the chaotic columnar region around the axis and that of the quasi-periodic core appear to increase and shrink, respectively, with increasing Reynolds number. On the

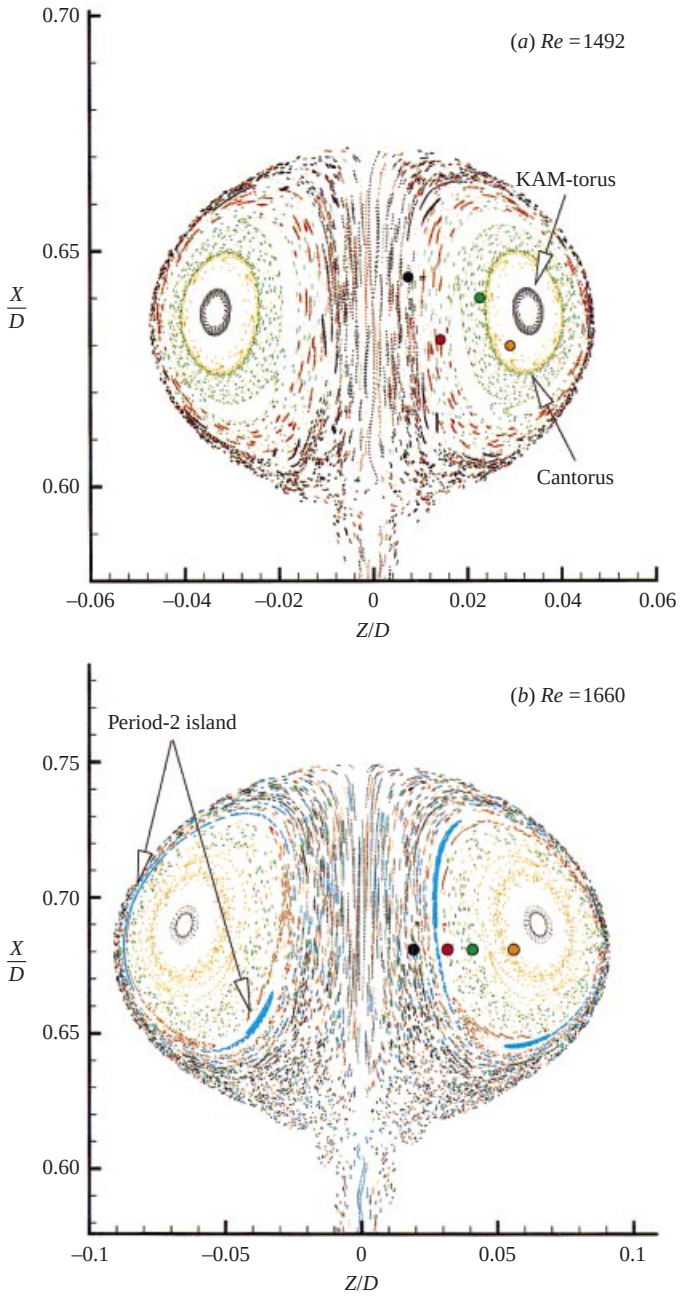

FIGURE 14. Poincaré sections for steady vortex breakdown bubbles in a container with $H/R = 2$. (*a*) $Re = 1492$; (*b*) $Re = 1667$. See caption of figure 12 for details on the construction of the two sections.

other hand, comparing figure 12 with figure 14 suggests significant variations both in the number and period of unmixed islands and in the permeability (or leakiness) of cantori with Reynolds number and aspect ratio. Three-dimensional KAM-theory should be able to explain the reasons for these variations. According to the theory (see Mezić & Wiggins 1994), the fate of the invariant tori of the axisymmetric flow

is, upon imposing a mild non-axisymmetric perturbation, determined by the ratio of two frequencies (see Fountain *et al.* 2000 for a comprehensive discussion): (i) the frequency of rotation on the diametral plane, Ω_ϕ, that describes the motion on planes that contain the axis; and (ii) the frequency of azimuthal rotation, Ω_θ, that describes the motion on planes perpendicular to the axis ($x = \text{const.}$). Tori for which the ratio $f = \Omega_\phi/\Omega_\theta$ is rational consist of periodic orbits whose period is equal to the denominator, say p, of the rational fraction f. Such tori are likely to break upon mild perturbation, leading to the formation of periodic islands surrounded by chaotic regions. On the other hand, tori for which f is sufficiently irrational (see Fountain *et al.* 2000 for the Diophantatine condition that needs to be satisfied for this to occur) consist of orbits that cover the entire torus ergodically and according to the theory many, although not necessarily the majority (see Mezić & Wiggins 1994), of such tori could survive mild perturbations. Fountain *et al.* (2000) were able to successfully apply these ideas to predict the period of the islands that formed upon mild perturbation of their flow field – a toroidal recirculating region generated by a tilted rotating disk fully submerged in a cylindrical container. Their results suggest that application of frequency analysis to the axisymmetric vortex breakdown flow fields should help explain the variations in the structure of periodic islands suggested by our computations. Such an undertaking, however, will be left as a topic for future research.

Finally, it is important to point out that the discussion presented in this and the previous sections clarifies the role of the various chaos-inducing mechanisms that are at work within stationary vortex breakdown bubbles. The Šil'nikov mechanism is responsible for breaking the invariance of the bubble-like surface and for the chaotic stirring of orbits within the columnar filament around the axis and the thin layer defining the outer surface of the bubble. The break-up of resonant tori and the KAM theorem, on the other hand, account for the rich dynamics in the internal toroidal region. Our computations suggest a general picture for this region, which consists of many periodic orbits of elliptic or hyperbolic type, homoclinic orbits to the hyperbolic orbits, invariant 2-tori around the elliptic ones, cantori and chaotic zones (Helleman 1980; MacKay 1994). That is, the dynamics in the interior of stationary vortex breakdown bubbles are entirely consistent with those of a mildly perturbed, volume-preserving toroidal flow and are accurately represented by Helleman's (1980) sketch of the phase-space dynamics of a perturbed Hamiltonian system.

7. Residence times of non-diffusive particles

As we discussed in § 5, particles re-circulate within the breakdown region for arbitrarily many times before finally exiting in a seemingly random sequence of bursting events (see figure 11). To explore this aspect of stationary vortex breakdown bubbles, we plot in figure 15 contours of constant residence time calculated from the trajectories of 10^4 particles. The particles were initially distributed axisymmetrically along a small disk of radius $0.01R$ centred around the axis just upstream of the breakdown bubble and their trajectories were integrated in time until every particle exited the bubble. For each particle, the residence time within the bubble is recorded and assigned to the particle's initial position on the release disk.

Figure 15 reveals a number of important new findings. First, we observe that particles that remain in the bubble the longest are organized in four spiral bands. This feature should be the result of the three-dimensionality of the approach vortex core. As we have already discussed, non-axisymmetric disturbances in the container flow grow inside the centrifugally unstable Stewartson layer, which loses stability in

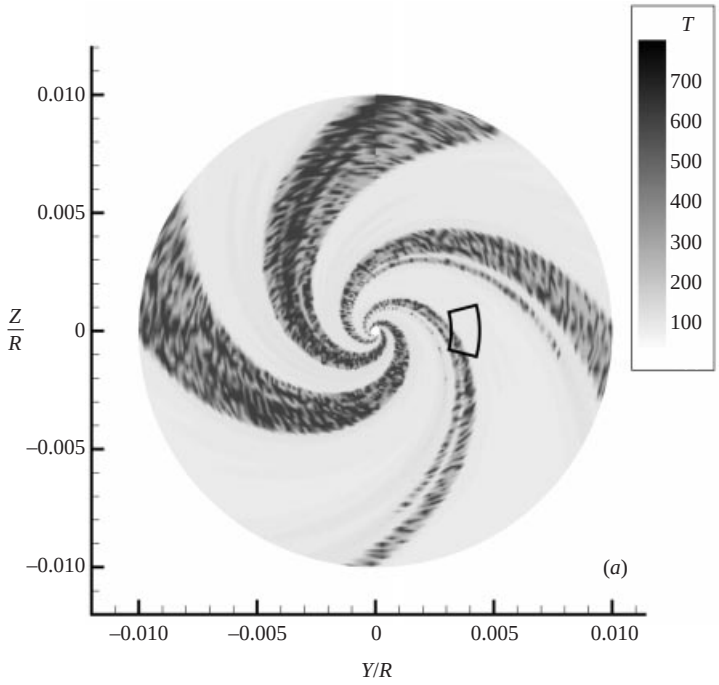

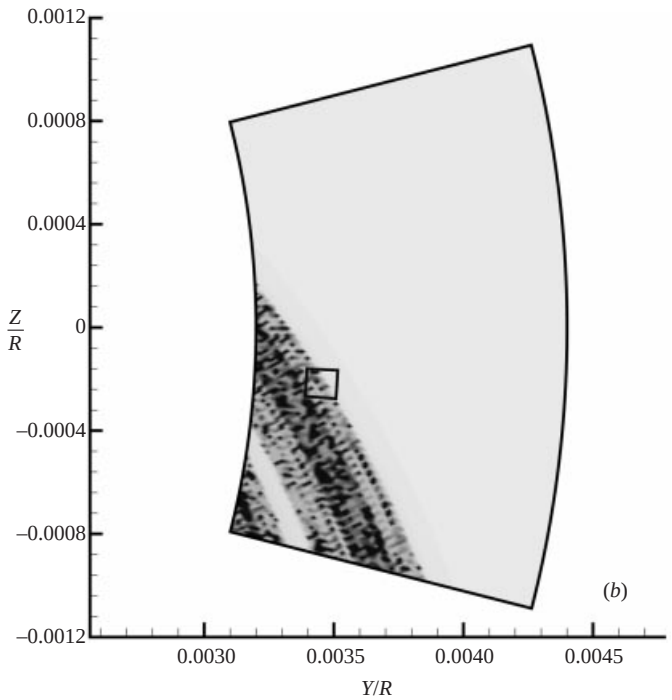

FIGURE 15 (*a*,*b*). For caption see page 284.

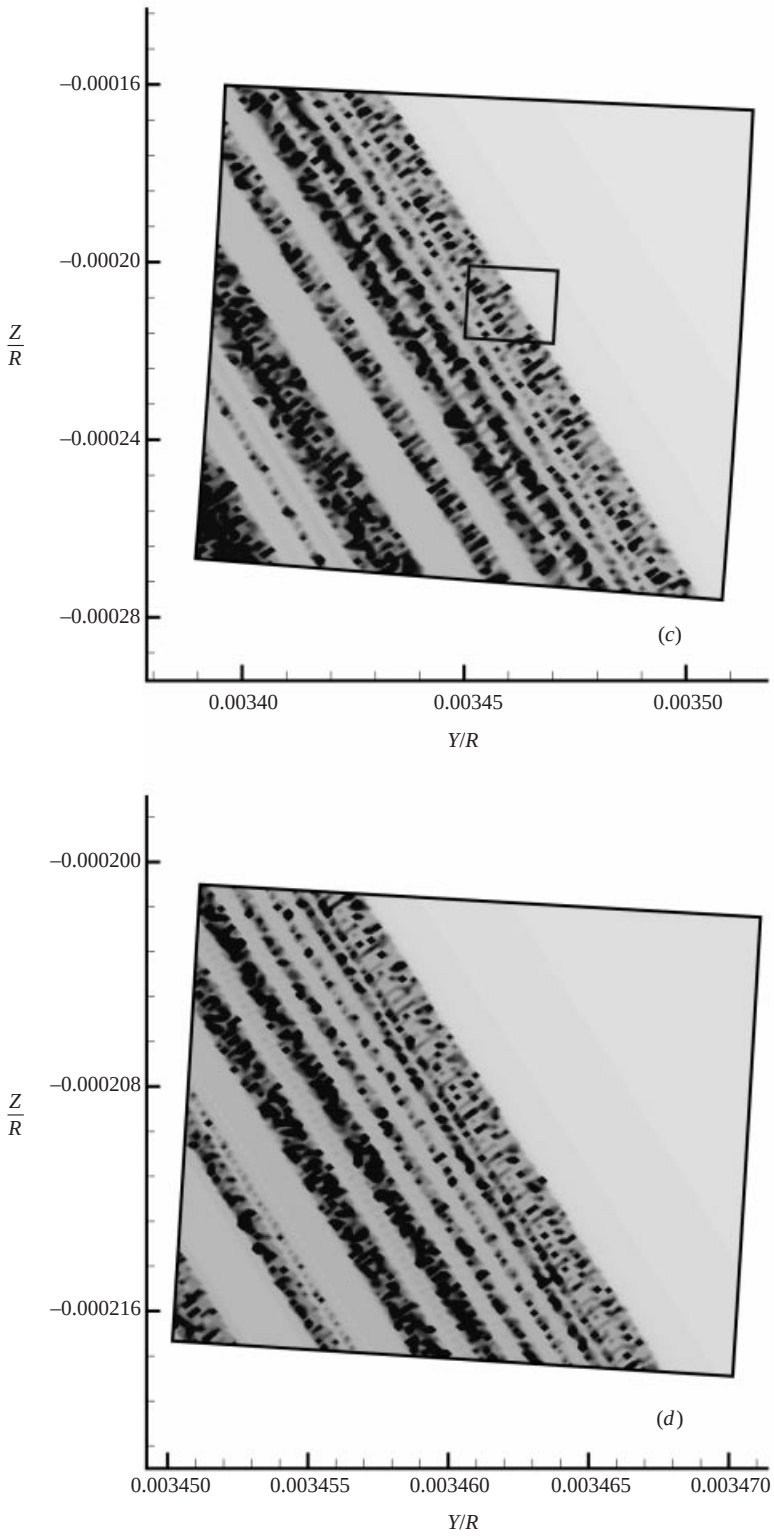

FIGURE 15. (*c*,*d*). For caption see page 284.

the form of four pairs of spiral vortices (Sotiropoulos & Ventikos 2001). Interestingly, however, there is a bias toward two of the four spirals that are considerably larger than the others. The most remarkable new finding perhaps is the internal composition of these four spiral regions as they appear to exhibit a distinct fractal-like structure. Clearly this is not a numerical artifact since in the small-residence-time regions of the map the contours do not exhibit this strange behaviour. To further investigate this issue, we repeat the same calculation by placing the 10^4 particles, which were initially spread along the entire disk, within successively smaller spatial regions as shown in figures 15(*b*) to 15(*d*). It is clear that as we increase the resolution at smaller scales, the resulting patterns begin to exhibit a self-similar fractal structure – notice that at the two smallest spatial scales we have zoomed in on, figures 15(*c*) and 15(*d*), the contour plots are practically identical. In fact it is evident that as we focus into smaller scales, additional bands of high residence times emerge continuously. These bands closely resemble fractal boundaries of basins of attraction for non-attracting chaotic sets and suggest a Cantor-set-like cross-section (Ott 1993). Their fractal structure is consistent with the chaotic nature of vortex breakdown flow fields and a direct manifestation of the extreme sensitivity of particle trajectories to arbitrarily small differences in initial conditions.

An important feature of the computed residence time map that is not directly apparent from the figure 15 is the fact that as we increase the resolution at smaller scales we uncover release points that lead to continuously increasing residence times. At the resolution of figure 15(*a*), the maximum residence time is approximately 700 non-dimensional units (corresponding to approximately 222 revolutions of the rotating lid), while at the resolution of figure 15(*d*), we have picked up points which lead to residence times as high as 7000 units (i.e. 2222 revolutions of the rotating lid). To demonstrate this feature, we show in figure 16 a plot similar to figure 15 but by including, at the two highest resolution levels, only contours that correspond to the very large residence times (the levels included in this plot range from 1000 to 7000). The resulting Cantor-dust-like contour plot strongly suggests that there exists a Cantor set of initial conditions (i.e. a set of measure zero but of finite dimension) that will lead to arbitrarily long residence times within the breakdown region. This conjecture is consistent with the chaotic nature of the flow and, in essence, is identical to the theoretical arguments made by Holmes (1984) that particles will re-circulate within the breakdown region for arbitrarily many times. Moreover, the concept of arbitrarily long residence times associated with a subset of measure zero (i.e. a Cantor set) of the total fluid flux into the bubble has already been introduced by MacKay (1994) in the context of the perturbed spheromak. MacKay (1994) also points out that the distribution of residence times within the bubble is 'likely to be highly non-trivial', a conjecture that is confirmed by the fractal structure we uncover herein. Finally, the existence of a Cantor set of initial conditions leading to arbitrarily long residence times within non-attracting chaotic sets, such as the volume-preserving vortex breakdown

FIGURE 15. Contours of residence time within the breakdown bubble plotted in terms of initial particle location. The extreme sensitivity to initial conditions and the fractal properties of this map become evident by increasing the resolution at smaller scales. For the first simulation (*a*), 10^4 particles were distributed along a disk of radius $0.01R$ located just upstream of the breakdown bubbles. For each of the other three simulations (*b*, *c*, and *d*), the 10^4 particles were released from successively smaller patches of the initial disk as indicated in each figure. The rotating lid completes one revolution in π time units. ($Re = 1850$, $H/R = 1.75$)

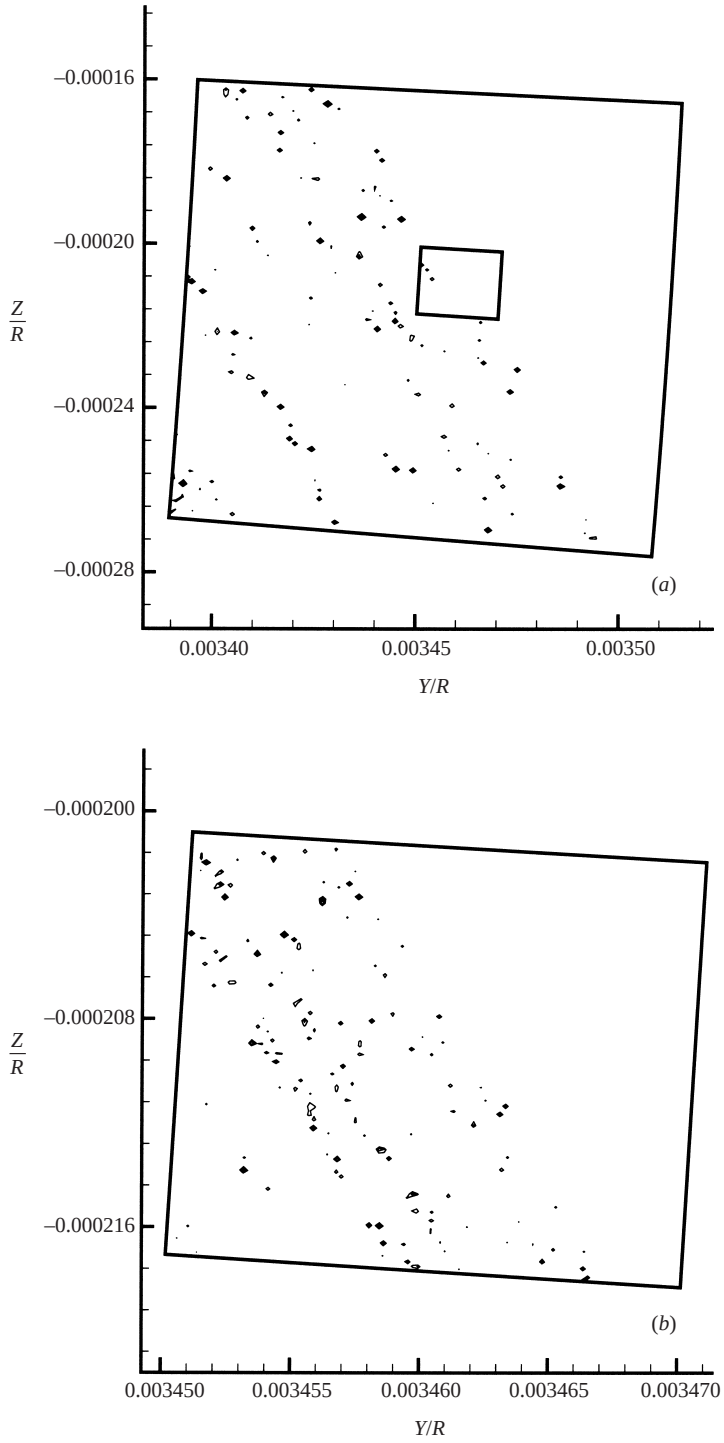

FIGURE 16. Contours of residence time as in figure 15(*c*, *d*). Only very large residence times (1000 to 7000 by 1000) are plotted to demonstrate the Cantor-dust-like structure of the resulting map.

flow field we study herein, is a well-documented phenomenon in studies of chaotic scattering (see Ott 1993 for a detailed review).

Experimental evidence suggesting very large residence times in vortex breakdown bubbles has been reported by Faler & Leibovich (1978) who visualized unsteady vortex breakdown bubbles in a straight circular diffuser. They observed that dye remained visible in the interior of the bubble for a considerable time after its supply was interrupted (see also Leibovich 1978). Preliminary flow visualization experiments we have recently carried out for the container flow point to similar conclusions. More specifically we have been able to observe the toroidal region in the interior of the bubble for extremely long times after the dye supply was interrupted (of the order of hundreds of lid revolutions). The results of these ongoing experiments will be reported in a future publication that is currently in preparation. We should emphasize, of course, that no arbitrarily long residence times are possible in the laboratory flow as molecular diffusion will ultimately cause the dye tracer to escape. In our simulations, however, arbitrarily long residence times associated with a Cantor set of initial conditions are possible as we are dealing with non-diffusive particles.

Finally, we should clarify what may appear at first glance to be a numerical paradox. The scales we have zoomed in on in figure 15 are much smaller than the size of the computational mesh we used to obtain the Eulerian flow field. It may, thus, appear odd that we find structure at such fine resolution. To clarify this paradox, recall the comments we made in § 3 above. There is a threshold spatial resolution that is required for the numerical method (Navier–Stokes solver) to yield an Eulerian velocity field that exhibits chaotic dynamics. After such a velocity field has been computed on a set of discrete nodes (the computational grid used to solve the Navier–Stokes equations), an interpolation scheme is used to produce a spatially 'continuous' velocity field required for the solution of the Lagrangian problem. The tri-linear spatial interpolation scheme we employ has been found adequate to preserve the chaotic dynamics of the computed discrete velocity field – recall our earlier discussion on numerical sensitivity in § 2. Since a chaotic flow field is characterized by extreme sensitivity to initial conditions, particles that are initially placed at a distance as small as the accuracy of the double-precision arithmetic we employ should diverge exponentially in time as they recirculate in the chaotic regime – and this does indeed happen. The scales we have zoomed in on in figure 15 are several orders of magnitude larger than the accuracy of the double-precision arithmetic we employ in the solution of the Lagrangian problem and, thus, the resulting fractal structure is well within the accuracy of our numerical scheme.

8. Emptying of a vortex breakdown bubble: the devil's staircase

In this section we further explore and quantify the emptying mechanism discussed in § 5, by calculating the rate at which a group of upstream-originating particles exits the bubble through the spiral-in saddle. We release the particles from a small disk, similar to that used to study the residence-time distributions in the previous section, and record the number of particles that remain inside the bubble at every instant in time until the last particle exits (see below for a clarification of this point). A particle is declared to have exited the bubble when it crosses a certain axial plane just downstream of the spiral-in saddle. Note that for a given set of upstream initial conditions, several particles do not enter the bubble and are, thus, the first to cross the 'exit' plane. These particles are omitted from the simulation. To investigate the sensitivity of the results presented herein to the size of the initial particle population,

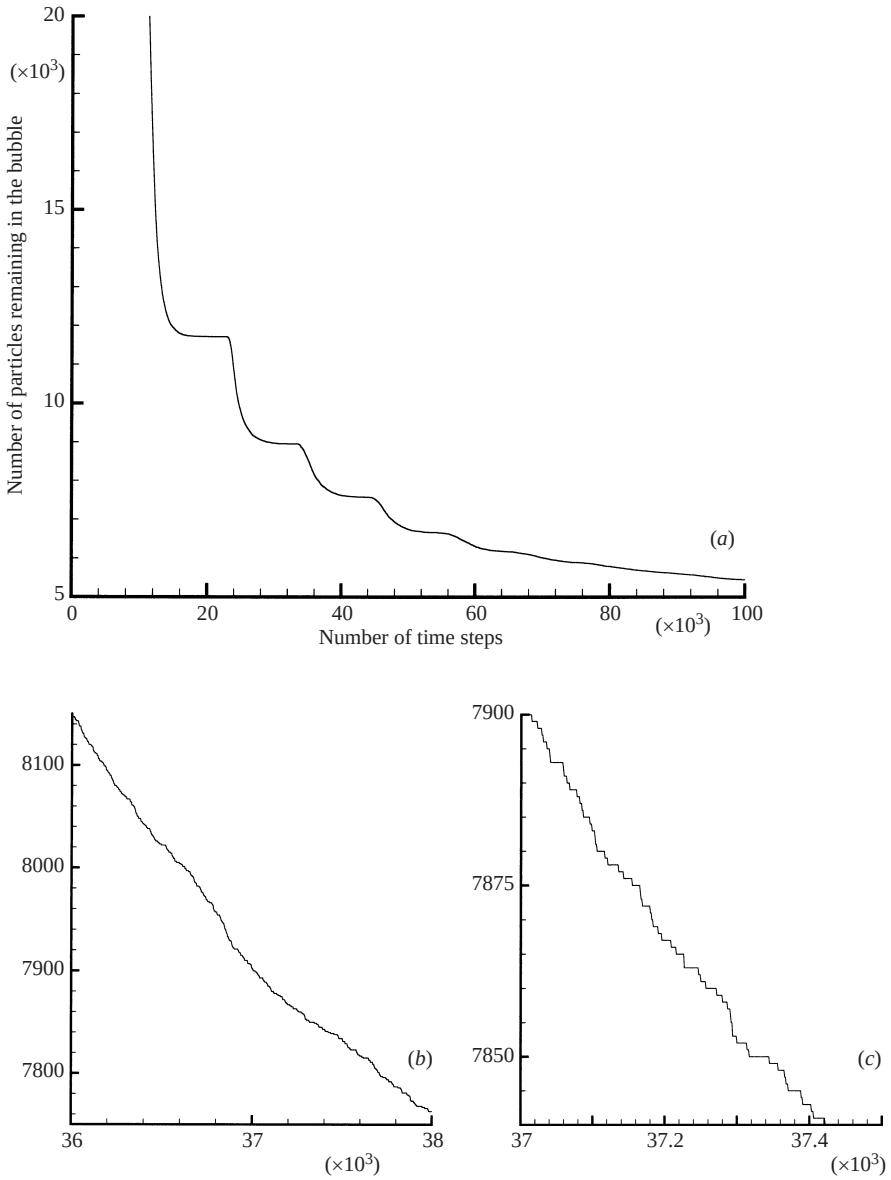

FIGURE 17. Emptying of a calculated stationary vortex breakdown bubble ($Re = 1850$, $H/R = 1.75$). 3×10^4 particles are distributed along a small disk located just upstream of the bubble. The number of particles remaining in the bubble is plotted as a function of time revealing a devil's staircase distribution. The self-similar nature of this curve is illustrated by zooming into smaller scales.

we have varied the particle number from $n = 10^3$ to 3×10^4 (see figure 18 below) – for each simulation, the particles were released from exactly the same small disk upstream of the vortex breakdown bubble. We have also investigated the effect of varying the size of the time increment used in the trajectory integration, by performing, for a fixed number of particles, simulations with successively smaller time steps. The results reported in this section are independent of the size of the time increment.

The computed temporal decay of an initial population of $n = 3 \times 10^4$ particles, for

the ($Re = 1850$, $H/R = 1.75$) vortex breakdown bubble, is plotted in figure 17. Note that the initial number of particles in the vertical axis is less than 3×10^4 because, as discussed above, particles that do not enter the bubble are omitted. A remarkable characteristic of the curve shown in figure 17 is that it is a piecewise continuous staircase-like structure, consisting of a series of horizontal plateaus each of seemingly random temporal duration. Furthermore, and as shown in figures 17(*b*) and (*c*), if part of the curve is magnified, the resulting curve looks very similar to the original one – curves with similar properties have been obtained for all simulated cases. Of course, and as clearly demonstrated in figure 17(*c*), magnification continues to reveal similarity at smaller scales until we reach the resolution of our discrete simulation.

The structure of the curve shown in figure 17 is strikingly similar to the so-called devil's staircase (Bak 1986), a fractal curve that has been found to emerge in a number of nonlinear systems, in both physics and engineering, undergoing a mode-locking transition to chaos. In such systems, the staircase has been shown to describe the dynamical behaviour as a function of frequency with the characteristic plateaus indicating locking at various rational frequencies (for specific examples see Bak 1986, Lacis *et al.* 1997, Reichhardt & Nori 1999). Recently Lai, Zyczkowski & Grebogi (1999) have shown that the devil-staircase characteristic is the universal behaviour in the parametric evolution of certain properties of chaotic saddles of nonlinear dynamical systems. The defining characteristic of the staircase, which also led to its name, is that between any two of its plateaus there is an infinite number of steps. Its mathematical construction is closely linked with the Cantor set and this relation is clearly evident in the computed curve shown in figure 17. Consider the time axis in this figure and remove all the intervals corresponding to fixed particle populations. What remains is a Cantor set, that is a set of points that has measure zero but, as we will subsequently show, finite fractal dimension. Of course a true Cantor set will be obtained in our case only in the limit of an infinite number of particles and as the time increment approaches zero.

Most of the physical applications of the staircase described in Bak (1986) involve dissipative systems with two competing frequencies where mode-locking occurs. In the present case, therefore, the devil's staircase emerges for the first time in an autonomous, three-dimensional, volume-preserving dynamical system that is spatially chaotic. The randomly varying lengths of its plateaus explain the emptying process of the breakdown bubble discussed previously in § 5. The initial particle population decays in time by sampling, as one would expect, all possible states, that is all integer numbers from the initial population to zero, but the temporal interval that the population remains fixed at a particular level varies randomly from level to level. Consequently the long plateaus would appear as pauses in the emptying process while a sequence of several consecutive short plateaus will result in what we previously described as a bursting event. We should emphasize that in the present simulation, with a finite set of discrete particles, the number of steps of the staircase cannot be infinite but rather equal to the total number of particles that enter the bubble in a given simulation. Only in the continuum limit would we anticipate that an initial tracer concentration will decay to zero by sampling, for random time intervals, the infinite sequence of all rational numbers between the initial concentration level and zero, thus yielding a true devil's staircase distribution.

In spite of the finite resolution we employ by specifying a fixed particle population, we can still demonstrate the fractal nature of the computed curve without having to perform simulations for an infinity of particles. To accomplish this, we calculate herein the fractal dimension of the Cantor set associated with the staircase shown

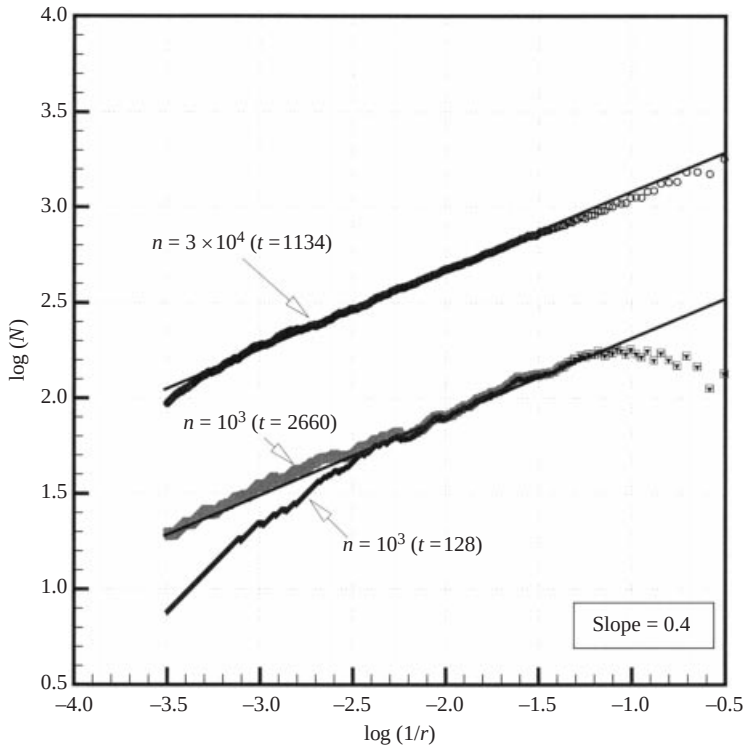

FIGURE 18. Fractal dimension of the Cantor set associated with the devil's staircase shown in figure 17. The number of particles used in the simulation is n and the simulated time interval for each case is t. The particles were distributed axisymmetrically along a small disk centred around the axis just upstream of the breakdown bubble. The slope of the straight line yields a fractal dimension $d = 0.4$.

in figure 17. The procedure we employ is that described in Bak (1986). We choose a given time interval r and calculate the total width $T(r)$ of all plateaus that are larger than r. We are interested in the space in between the plateaus, $T_{max} - T(r)$, which eventually shrinks into a Cantor set (T_{max} is the maximum residence time in our discrete simulation). To measure this space we define the total number N of 'holes' of size r, given by

$$N(r) = \frac{T_{max} - T(r)}{r}. \tag{8.1}$$

If the variation of $N(r)$ versus $1/r$ on a log–log scale is linear, then

$$N(r) \approx (1/r)^d \tag{8.2}$$

where d is the slope of the resulting straight line. That is, the space between the plateaus vanishes as r^{1-d} at $r \to 0$ and the devil's staircase is complete (Bak 1986). The exponent d is the fractal dimension of the Cantor set, which is complementary to the set of plateaus comprising the devil's staircase.

In figure 18, we plot on a log–log scale N vs. $1/r$ for the two staircases obtained from the $n = 10^3$ and $n = 3 \times 10^4$ simulations, respectively. We include both of these simulations in order to explore the sensitivity of the so-computed fractal dimension to the number of initial particles. For both simulations, we find that a straight line with

slope $d = 0.4$ fits well all points over a broad range of plateau sizes – approximately 2.3 and 3.0 orders of magnitude variation in r for the $n = 10^3$ and $n = 3 \times 10^4$ cases, respectively. Note, however, that increasing the number of particles results in dramatic improvements for small values of r and in smoother overall linear variation. We should also note and comment on the apparent departure of the calculated points for the $n = 3 \times 10^4$ case from the linear variation as r approaches large values (see figure 18). This trend is an artifact of our incomplete, for this case, numerical simulation. Due to the asymptotic nature of the curve shown in figure 17, larger plateaus tend to appear more frequently when relatively few particles remain in the bubble. Since many of these last remaining particles could have arbitrarily long residence times (see previous section), continuation of the time integration long enough for all particles to exit requires excessive computational resources – especially for the large number of particles used in this refined simulation. For that reason we had to terminate the particle integration when approximately 4000 particles were still remaining in the interior of the bubble. Consequently, the so-computed staircase does not contain sufficiently many large size plateaus for the linear variation of N to be sustained at larger r. To prove that this is indeed the reason for the observed departure from linearity, we also include in figure 18 the curve that resulted when the $n = 10^3$ simulation, which was actually carried out until all particles exited ($t = 2660$), was terminated at a much earlier time ($t = 128$) – only 100 particles were left inside the bubble at $t = 128$ and, thus, more than 2500 s of additional simulation were required for these few remaining particles to exit. Clearly, reducing the integration time results in the same departure from linear variation at larger values of r as that observed for the $n = 3 \times 10^4$ simulation. This small discrepancy not withstanding, figure 18 provides conclusive evidence that the curve shown in figure 17 is a complete devil's staircase with fractal dimension $d = 0.4$. Interestingly, this value of the fractal dimension is lower than the $d = 0.87$ 'universal' constant (Bak 1986) that has been previously found in a number of dissipative dynamical systems undergoing mode-locking transition to chaos.

To further explore the statistical properties of the devil's staircase curve, we plot in figure 19 the calculated (for the staircase shown in figure 17) frequency of occurrence, $S(r)$, of the various plateau sizes (i.e. the waiting times between bursting events) as a function of the plateau size r – i.e. the histogram of r. Figure 19 shows that the frequency of occurrence diminishes monotonically as the plateau size increases. Furthermore, a power law of the form

$$S(r) \approx (1/r)^a \tag{8.3}$$

with $a = 1.4$ appears to fit well the computed data points. Note that a power-law distribution for S is consistent with the nature of the devil's staircase, as plateau sizes of zero length correspond to the points of the complementary Cantor set and should, thus, be infinitely many. It is also important to point out that the apparent relation between the fractal dimension d and the exponent a ($a = 1 + d$) is not coincidental. Assuming a continuous function $S = S(r)$ of the form given by equation (8.3) and noting that $T(r)$ (the total length of plateaus with size greater than r) can be computed from S as follows (r_{max} is the size of the largest plateau):

$$T(r) = \int_r^{r_{max}} r' S(r')\, \mathrm{d}r', \tag{8.4}$$

we can easily show that the number of holes N of size r defined by equation (8.2) is

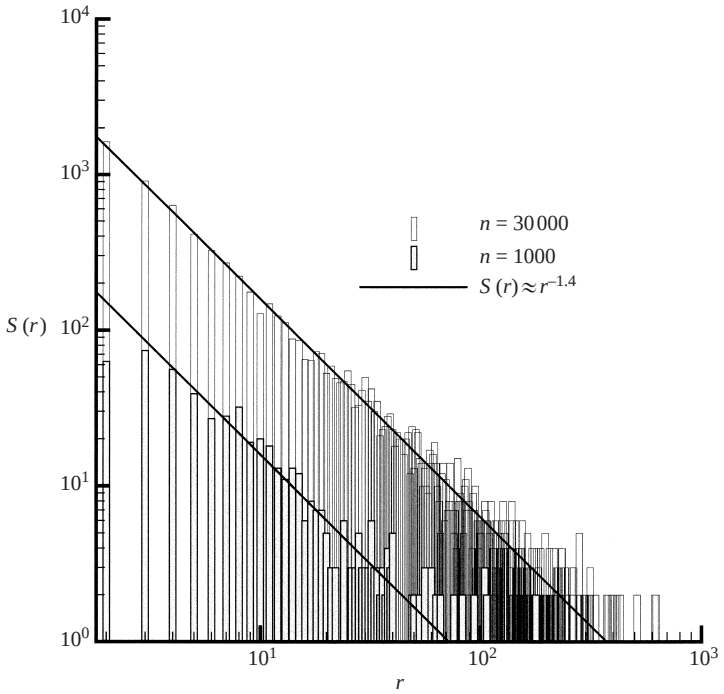

FIGURE 19. Histogram of the staircase plateau sizes (waiting times between consecutive bursts) for the ($Re = 1850$, $H/R = 1.75$) vortex breakdown bubble. The two histograms shown were extracted from the same staircases used to calculate the fractal dimension in figure 18, with 10^3 and 3×10^4 particles, respectively. The continuous line is the power-law distribution that was obtained from the 3×10^4-particle simulation. Even though the unresolved simulation (10^3 particles) yields a very noisy histogram, the same power-law appears to fit reasonably well over a considerable range of r values.

given by the following equation:

$$N = \frac{1}{r}\int_0^r r' S(r')\,\mathrm{d}r' \approx \left(\frac{1}{r}\right)^{a-1}. \tag{8.5}$$

Comparison with equation (8.2) yields the relation implied by the numerical values in figures 18 and 19, i.e. $d = a - 1$. In other words, the fractal dimension of the complementary Cantor set can also be calculated from the histogram of plateau sizes.

To investigate whether the fractal dimension of the devil's staircase is universal for this problem or varies with the governing parameters of the flow (H/R and Re), we carried out computations similar to those described above but for the two bubbles shown in figure 14 ($Re = 1492$ and 1667 for $H/R = 2$). For both simulations we used 3×10^4 particles and obtained staircase-like curves such as the one shown in figure 17. We also found that the fractal dimension d decreases with Reynolds number from 0.65, for $Re = 1492$, to 0.55, for $Re = 1667$. Although these results suggest that the fractal dimension is a strong function of H/R and Re, the few cases we have considered thus far do not allow us to establish any meaningful trends. Computations over a much broader range of Reynolds numbers and aspect ratios will be needed before such trends can be extracted with certainty.

Finally, we should point out that our findings in this and the previous sections point to the conclusion that the infinite intersections of the stable and unstable manifolds

of the spiral-in saddle, through which upstream-originating particles enter and exit that bubble, exhibit a fractal spatial structure. Since chaotic Šil'nikov orbits will have to exit through this fractal 'window', their exit time will be extremely sensitive to arbitrarily small differences in the particle initial location, and, thus, the resulting fractal structure in the residence time maps and the variations in the sizes of the devil's staircase plateaus.

9. Summary and concluding remarks

We have investigated computationally the dynamics of particle paths within three-dimensional, stationary, vortex breakdown flow fields in a closed cylindrical container with a rotating lid. By demonstrating that the upstream and downstream fixed hyperbolic points of a vortex breakdown bubble are of spiral focus type, we argued that the Šil'nikov mechanism is responsible for the destruction of the invariant axisymmetric bubble surface and the chaotic stirring of upstream-originating particles (Šil'nikov's 1965). We constructed Poincaré sections to clarify the rich dynamics of the flow in the interior of vortex breakdown bubbles. The picture that emerged is consistent with what we would generically anticipate for a perturbed, three-dimensional, volume-preserving system. The dynamics are characterized by a sequence of nested KAM-tori and cantori with the gaps between adjacent tori populated by periodic islands embedded within large regions of chaotic motion. We calculated residence times of non-diffusive Lagrangian tracers and argued that there exists a Cantor set of initial conditions leading to arbitrarily long residence times within the breakdown region. We also showed that the rate at which upstream originating particles exit the breakdown region exhibits a devil's staircase distribution. The fractal nature of this curve was established rigorously by computing the fractal dimension of the Cantor set associated with its construction. We presented results for two aspect ratios and a total of three Reynolds numbers, which show that the chaotic dynamics within the bubble (number of un-mixed islands and the extent of the chaotic and quasi-periodic regions) and the fractal dimension of the devil's staircase depend strongly on the Reynolds number and container aspect ratio.

Holmes's (1984) ingenious prediction of a spatially chaotic flow field in which particles enter the breakdown region and recirculate arbitrarily many times before they finally exit, is essentially the type of Lagrangian motion we find herein. An important difference between our findings and Holmes's arguments is that he discussed the effects of an arbitrarily small, time-periodic, non-axisymmetric mode on a steady, axisymmetric vortex breakdown bubble. Our results, on the other hand, suggest that even stationary non-axisymmetric perturbations suffice to drastically alter the integrable dynamics of the axisymmetric flow and lead to the onset of chaotic particle paths. It is important to recognize that such a scenario is not new in the dynamical systems literature. Its theoretical foundations, in the context of an autonomous, three-dimensional, dynamical system whose dynamics closely mimic those of a stationary vortex breakdown bubble, were first laid out by Broer & Vegter (1984) – see also the more recent discussion in Wiggins (1990). Our results are also entirely consistent with the more recent theoretical predictions by MacKay (1994). His descriptions of the manifold structure and internal dynamics of the perturbed stationary spherical vortex are essentially identical to those derived from our computations for three-dimensional, stationary vortex breakdown bubbles (McKay 1994). Interestingly, MacKay (1994) also discussed the possibility of highly complex distributions of residence times and alluded to the existence of a subset of measure

zero of the total flux into the bubble that is associated with arbitrarily long residence times.

Our work, along with our earlier contribution (Sotiropoulos & Ventikos 2001) and the recent experimental study of Spohn *et al.* (1998), clarify the origin of the asymmetries observed in all laboratory visualization experiments and resolve conclusively the fifteen-year old controversy regarding the fundamental nature of the bubble-type mode of vortex breakdown in the container problem. The asymmetric folds that invariably appear at the downstream end of the bubble (see, among others, Escudier 1984; Fujimura, Koyama & Hyun 1995; Spohn *et al.* 1998) are due to the very complex topology of trajectories in the vicinity of the spiral-in saddle. Moreover, the spiral deflection of the dye filament at the upstream end of the bubble is not an artifact of the visualization technique, as has been repeatedly argued in the literature (Stevens *et al.* 1999), but the projection on a diametral plane of the unstable manifolds of the spiral-out saddle.

The present computational findings in conjunction with previous theoretical work in the area of nonlinear dynamical systems (Broer & Vetger 1984; Wiggins 1990; MacKay 1994) explain clearly the reason why previous axisymmetric computations have succeeded in predicting most Eulerian features of the flow reasonably well (e.g. Lopez 1990; Gelfgat *et al.* 1996; Brons *et al.* 1999). The non-axisymmetric component of the flow in the vicinity of real-life vortex breakdown bubbles is indeed very small and, thus, the Eulerian flow can be approximated well by the axisymmetric assumption. Yet this small three-dimensional perturbation has a profound effect on the Lagrangian characteristics of the flow. In other words, even though the real-life and ideal (axisymmetric) flow fields are very similar from the Eulerian standpoint, their Lagrangian descriptions are as fundamentally different as order and chaos.

Our findings concerning the fractal structure of the residence-time maps and the devil's staircase, which essentially confirm and help clarify Holmes's and MacKay's theoretical predictions, are both spectacular examples of the physical relevance of the Cantor set. Note, for instance, that the concept of arbitrarily long residence times appears counter-intuitive from the standpoint of conservation of volume in an incompressible fluid. Yet when linked to a Cantor-set of release conditions, this apparent physical contradiction is removed. By definition a Cantor set is not dense at any interval, and, thus, the total tracer flow rate that emanates from points leading to arbitrarily long residence times is in fact zero.

There are numerous aspects of the Lagrangian dynamics of steady vortex breakdown bubbles we have uncovered herein that require further investigation. Extensive parametric studies, over a broad range of aspect ratios and Reynolds numbers, should be carried out to explore and quantify the dependence of the dynamics in the interior of the bubbles and the fractal properties of residence-time distributions on Reynolds number and aspect ratio. Results from these studies could help validate recent theories that have linked the extent of chaotically advected regions in wall-bounded flows with the Reynolds number of the flow and the thickness of the wall boundary layers (Mezić 2001). They should also provide a useful test-bed for testing and further refining the predictive capabilities of three-dimensional KAM theory (see Fountain *et al.* 2000). By identifying and quantifying links between Lagrangian transport and the physics of the flow, results from such studies could also lead to rational strategies for controlling chaotic stirring and residence times of particles within the breakdown region. Such quantitative parametric investigation is currently under way and its results will be reported in a future communication.

We thank Greg King, Igor Mezić, Thanasis Yannacopoulos, and the anonymous referees for several useful comments and suggestions that greatly improved the manuscript. The computations were performed on the Cray T-90 supercomputer of the San Diego Supercomputer Centre and the multiprocessor Silicon Graphics Origin 2000 system of the Office of Information Technology at the Georgia Institute of Technology. F. S. was partly supported by NSF grant CMS-9875691.

REFERENCES

Anderson, P. D., Galaktionov, O. S., Peters, G. W. M., Van de Vosse, F. N. & Meijer, H. E. H. 1999 Analysis of mixing in three-dimensional time-periodic cavity flows. *J. Fluid Mech.* **386**, 149–166.

Aref, H. 1984 Stirring by chaotic advection. *J. Fluid Mech.* **143**, 1–21.

Aref, H. 1999 Order in chaos. *Nature* **401**, 756–757.

Arneodo, A., Coullet, P. & Tresser, C. 1982 Oscillators with chaotic behavior: an illustration of a theorem by Šil'nikov. *J. Statist. Mech.* **27**, 171–182.

Arnold, V. I. 1965 Sur la topologie des ecoulements stationaries des fluides parfaits. *C. R. Acad. Sci. Paris* **261**, 17–20.

Ashwin, P. & King, G. P. 1995 Streamline topology in eccentric Taylor vortex flow. *J. Fluid Mech.* **285**, 215–247.

Ashwin, P. & King, G. P. 1997 A study of particle paths in non-axisymmetric Taylor-Couette flows. *J. Fluid Mech.* **133**, 341–362.

Bajer, K. & Moffatt, H. K. 1990 On a class of steady confined Stokes flows with chaotic streamlines. *J. Fluid Mech.* **212**, 337–363.

Bak, P. 1986 The devil's Staircase. *Physics Today*, **39**(12), 38–45.

Beige, D., Leonard, A. & Wiggins S. 1994 Invariant manifold templates for chaotic advection. *Chaos, Solitons, and Fractals* **4**(6), 749–868.

Broer, H. W. & Vegter, G. 1984 Subordinate Šil'nikov bifurcations near some singularities of vector fields having low codimension. *Ergod. Theor. Dyn. Syst.* **4**, 509–525.

Broomhead, D. S. & King, G. P. 1986 On the qualitative analysis of experimental dynamical systems. In *Nonlinear Phenomena and Chaos* (ed. S. Sarkar). Adam Hilger, Bristol.

Brons, M., Voigt, L. K. & Sorensen, J. N. 1999 Streamline topology of steady axisymmetric vortex breakdown in a cylinder with co- and counter-rotating, end-covers. *J. Fluid Mech.* **401**, 275–292.

Brown, G. L. & Lopez, J. M. 1990 Axisymmetric vortex breakdown. Part 2. Physical mechanisms. *J. Fluid Mech.* **221**, 553–576.

Buchanan, J. L. & Turner. P. R. 1992 *Numerical Methods and Analysis.* McGraw-Hill.

Cartwright, J. H. E., Feingold, M. & Piro, O. 1996 Chaotic advection in three-dimensional unsteady incompressible laminar flow. *J. Fluid Mech.* **316**, 259–284.

Chaiken, J., Chevray, R., Tabor, M. & Tan, Q. M. 1986 Experimental study of Lagrangian turbulence in Stokes flow. *Proc. R. Soc. Lond.* A **408**, 165–174.

Chen, R.-H. & Driscoll, J. F. 1988 The role of the recirculation vortex in improving fuel-air mixing within swirling flames. *22nd Intl Symp. on Combustion*, pp. 531–540. The Combustion Institute.

Chien, W.-L., Rising, H. & Ottino, J. M. 1986 Laminar mixing and chaotic mixing in several cavity flows. *J. Fluid Mech.* **170**, 355–377.

Dombre, T., Frisch, U., Green, J. M., Henon, M., Mehr, A. & Soward, A. M. 1986 Chaotic streamlines in ABC flows. *J. Fluid Mech.* **167**, 353–391.

Escudier, M. P. 1984 Observations of the flow produced in a cylindrical container by a rotating endwall. *Exps. Fluids* **2**, 189–196.

Escudier, M. P. 1988 Vortex breakdown: observations and explanations. *Prog. Aerospace Sci.* **25**, 189–229.

Faler, J. H. & Leibovich, S. 1977 Disrupted states of vortex flow and vortex breakdown. *Phys. Fluids* **20**, 1385–1400.

Faler, J. H. & Leibovich, S. 1978 An experimental map of the internal structure of a vortex breakdown. *J. Fluid Mech.* **86**, 313–335.

Feikema, D., Chen, R.-H. & Driscoll, J. F. 1990 Enhancement of flame blowout limits by the use of swirl. *Combust. Flame* **80**, 183–195.

Feingold, M., Kadanoff, L. P. & Piro, O. 1988 Passive scalars, three-dimensional volume-preserving maps, and chaos. *J. Statist. Phys.* **50**, 529–565.

Fountain, G. O., Khakhar, D. V., Mezić, I. & Ottino, J. M. 2000 Chaotic mixing in a bounded three-dimensional flow. *J. Fluid Mech.* **417**, 265–301.

Fountain, G. O., Khakhar, D. V. & Ottino, J. M. 1998 Visualization of three-dimensional chaos. *Science* **281**, 683–686.

Fujimura, K., Koyama, H. S. & Hyun, J. M. 1997 Time-dependent vortex breakdown in a cylinder with a rotating lid. *Trans. ASME: J. Fluids Engng* **119**, 450–453.

Gaspard, P. & Nicolis, G. 1983 What can we learn from homoclinic orbits in chaotic dynamics? *J. Statist. Phys.* **31**, 499–518.

Gelfgat, A. Yu., Bar-Yoseph, P. Z. & Solan, A. 1996 Stability of confined flow with and without vortex breakdown. *J. Fluid Mech.* **311**, 1–36.

Ghosh, S., Leonard, A. & Wiggins, S. 1998 Diffusion of a passive scalar from a no-slip boundary into a two-dimensional chaotic advection field. *J. Fluid Mech.* **372**, 119–163.

Glendinning, P. & Sparrow, C. 1986 T-Points: a codimension two heteroclinic bifurcation. *J. Statist. Phys.* **43**, 479–488.

Haller, G. & Mezić, I. 1998 Reduction of three-dimensional, volume-preserving flows by symmetry. *Nonlinearity* **11**, 319–339.

Healey, J. J., Broomhead, D. S., Cliffe, K. A., Jones, R. & Mullin, T. 1991 The origins of chaos in a modified Van der Pol oscillator. *Physica* D **48**, 322–339.

Helleman, R. H. G. 1980 Self-generated chaotic behavior in non-linear mechanics. In *Fundamental Problems in Statistical Mechanics*, Vol. 5 (ed. E. G. D. Cohen), pp. 165–233. North Holland.

Hénon, M. 1966 Sur la topologie des lignes de courant dans un cas Particulier. p *C. R. Acad. Sci. Paris* A **262**, 312–314.

Hobbs, D. M. & Muzzio, F. J. 1997 The Kenics static mixer. A three-dimensional chaotic flow. *Chem. Engng J.* **67**, 153–166.

Hobbs, D. M. & Muzzio, F. J. 1998 The curvature of material lines in a three-dimensional chaotic flow. *Phys. Fluids* **10**, 1942–1952.

Holm, D. D. & Kimura, Y. 1991 Zero-helicity kinematics of three-dimensional advection. *Phys. Fluids* A **3**, 1033–1038.

Holmes, P. 1984 Some remarks on chaotic particle paths in time-periodic, three-dimensional swirling flows. *Contemp. Maths* **28**, 393–404.

Hourigan, K., Graham, L. J. W. & Thompson, M. C. 1995 Spiral streaklines in pre-vortex breakdown regions of axisymmetric swirling flows. *Phys. Fluids* **7**, 3126–3128.

Jackson, E. A. 1991 *Perspectives of Nonlinear Dynamics 2.* Cambridge University Press.

Jones, S. W., Thomas, O. M. & Aref, H. 1989 Chaotic advection by laminar flow in a twisted pipe. *J. Fluid Mech.* **209**, 335–357.

Khakhar, D. V., Franjione, J. G. & Ottino, J. M. 1987 A case study of chaotic mixing in deterministic flows. The partitioned pipe mixer. *Chem. Engng Sci.* **42**, 2909–2926.

Khakhar, D. V., Rising, H. & Ottino, J. M. 1986 An analysis of chaotic mixing in two chaotic flows. *J. Fluid Mech.* **172**, 419–451.

Kroujiline, D. & Stone H. A. 1999 Chaotic streamlines in steady bounded three-dimensional Stokes flows. *Physica* D **130**, 105–132.

Kusch, H. A. & Ottino, J. M. 1992 Experiments on mixing in continuous chaotic flows. *J. Fluid Mech.* **236**, 319–348.

Lacis, S., Barci, J. C., Cebers, A. & Perzynski, R. 1997 Frequency locking and devil's staircase for a two-dimensional ferrofluid droplet in an elliptically polarized rotating magnetic field. *Phys. Rev.* E **55**, 2640–2648.

Lai, Y.-C., Zyczkowski, K. & Grebogi, C. 1999 Universal behavior in the parametric evolution of chaotic saddles. *Phys. Rev.* E **59**, 5261–5265.

Leibovich, S. 1978 The structure of vortex breakdown.*Ann. Rev. Fluid Mech.* **10**, 221–246.

Leibovich, S. 1984 Vortex stability and breakdown: Survey and extension. *AIAA J.* **22**, 1192–1206.

Leong, C. W. & Ottino, J. M. 1989 Experiments on mixing due to chaotic advection in a cavity. *J. Fluid Mech.* **209**, 463–499.

Lopez, J. M. 1990 Axisymmetric vortex breakdown. Part 1. Confined swirling flow. *J. Fluid Mech.* **221**, 533–552.

Lopez, J. M. & Perry, A. D. 1992 Axisymmetric vortex breakdown. part 3: onset of periodic flow and chaotic advection. *J. Fluid Mech.* **234**, 449–471.

Lucas, K. V. 1997 Numerical investigation of three-dimensional vortex breakdown. PhD Thesis, Dept. of Aeronautics and Astronautics, Stanford University, Palo Alto, CA.

Mackay, R. S. 1994 Transport in 3D volume-preserving flows. *J. Nonlinear Sci.* **4**, 329–354.

Mackay, R. S., Meiss, J. D. & Percival, I. C. 1984 Transport in Hamiltonian systems. *Physica* D **13**, 55–81.

Mezić, I. 2001 Three-dimensional chaotic advection in bounded Navier–Stokes flows. *J. Fluid Mech.* **431**, 347–370.

Mezić, I., Leonard, A. & Wiggins, S. 1998 Regular and chaotic particle motion near a helical vortex filament. *Physica* D **111** 1–4, 179–201.

Mezić, I. & Wiggins, S. 1994 On the integrability and perturbation of three-dimensional fluid flows with symmetry. *J. Nonlinear Sci.* **4**, 157–194.

Mullin, T. 1993 A multiple bifurcation point as an organizing centre for chaos. In *The Nature of Chaos* (ed. T. Mullin), pp. 51–68. Oxford University Press.

Mullin, T. & Price, T. J. 1989 An experimental observation of chaos arising from the interaction of steady and time-dependent flows. *Nature* **340**, 294–296.

Murman, E. M. & Powell, K. G. 1989 Trajectory integration in vortical flows. *AIAA J.* **27**, 982.

Neitzel, G. P. 1988 Streak-line motion during steady and unsteady axisymmetric vortex breakdown. *Phys. Fluids* **31**, 958–960.

Ott, E. 1993 *Chaos in Dynamical Systems*. Cambridge University Press.

Ottino, J. M. 1989 *The Kinematics of Mixing: Stretching, Chaos, and Transport*. Cambridge University Press.

Pao, H.-P. 1970 A numerical computation of a confined rotating flow. *Trans. ASME E: J. Appl. Mech.* **37**, 480–487.

Peacock, T., Mullin, T. & Binks, D. J. 1999 Bifurcation phenomena in flows of a nematic liquid crystal. *Intl J. Bifurcation Chaos* **9**, 427–441.

Reichhardt, C. & Nori, F. 1999 Phase locking, devil's Staircase, Farey Tress, Arnold tongues in driven vortex lattices with periodic pinning. *Phys. Rev. Lett.* **82**, 414–417.

Rom-Kedar, V., Leonard, A. & Wiggins, S. 1990 An analytical study of transport, mixing, and chaos in an unsteady vortical flow. *J. Fluid Mech.* **214**, 347–394.

Rothstein, D., Henry, E. & Gollub, J. P. 1999 Persistent patterns in transient chaotic fluid mixing. *Nature* **401**, 770–772.

Rudman, M. 1998 Mixing and particle dispersion in the wavy vortex regime of Taylor-Couette flow. *AIChE J.* **44**, 1015–1026.

Rudolph, M., Shinbrot, T. & Lueptow, R. M. 1998 A model of mixing and transport in wavy Taylor-Couette flow. *Physica* D **121**, 163–174.

Sarpkaya, T. 1971 On stationary and travelling vortex breakdowns. *J. Fluid Mech.* **45**, 545–559.

Šil'nikov 1965 A case of the existence of a denumerable set of periodic motions. *Sov. Math. Dokl.* **6**, 163–166.

Sorensen, J. N. & Christensen, E. A. 1995 Direct numerical simulation of rotating fluid flow in a closed cylinder. *Phys. Fluids* **7**, 764–778.

Sotiropoulos, F. & Ventikos, Y. 1998 Transition from bubble-type vortex breakdown to columnar vortex in a confined swirling flow. *Intl J. Heat Fluid Flow* **19**, 446–458.

Sotiropoulos, F. & Ventikos, Y. 2001 The three-dimensional structure of confined swirling flows with vortex breakdown. *J. Fluid Mech.* **426**, 155–157.

Spall, R. E. & Gatski, T. B. 1991 A computational study of the topology of vortex breakdown. *Proc. R. Soc. Lond.* A **435**, 321–337.

Spohn, A., Mory, M. & Hopfinger, E. J. 1993 Observations of vortex breakdown in an open cylindrical container with rotating bottom. *Exps. Fluids* **13**, 70–77.

Spohn, A., Mory, M. & Hopfinger, E. J. 1998 Experiments on vortex breakdown in a confined flow generated by a rotating disk. *J. Fluid Mech.* **370**, 73–99.

Stone, H. A., Nadim, A. & Strogatz, S. H. 1991 Chaotic streaklines inside drops immersed in steady linear flows. *J. Fluid Mech.* **232**, 629–646.

Stevens, J. L., Lopez, J. & Cantwell, B. J. 1999 Oscillatory flow states in an enclosed cylinder with a rotating endwall. *J. Fluid Mech.* **389**, 101–118.

Swanson, P. D. & Ottino, J. M. 1990 A comparative computational and experimental study of chaotic mixing of viscous fluids. *J. Fluid Mech.* **213**, 227–249.

Tromp, J. C. & Beran P. S. 1997 The role of non-unique axisymmetric solutions in 3-D vortex breakdown. *Phys. Fluids* **9**, 992–1002.

Tsitverblit, N. & Kit, E. 1998 On the onset of unsteadiness in confined vortex flows. *Fluid Dyn. Res.* **23**(3), 125–152

Watson, J. P. & Neitzel, G. P. 1996 Numerical evaluation of a vortex-breakdown criterion. *Phys. Fluids* **8**, 3063–3071.

Wiggins, S. 1990 *Introduction to Applied Nonlinear Dynamical Systems and Chaos.* Texts in Applied Mathematics, Vol. 2. Springer.

Yannacopoulos, A. N., Mezić, I., Rowlands, G. & King, G. P. 1998 Eulerian diagnostics for Lagrangian chaos in three-dimensional Navier–Stokes flows. *Phys. Rev.* E **57**, 482–490.

Zheligovsky, V. A. 1993 A kinematic magnetic dynamo sustained by a Beltrami flow in a sphere. *Geophys. Astrophys. Fluid Dyn.* **73**, 217–254.